A CLOUD CHAMBER INVESTIGATION OF INTERACTIONS AT ENERGIES GREATER THAN 50 BEV

Thesis by

Earl Donald Jacobs

In Partial Fulfillment of the Requirements

For the Degree of

Doctor of Philosophy

California Institute of Technology

Pasadena, California

1961

ACKNOWLEDGEMENTS

It is a pleasure to acknowledge the all important guidance and supervision of Professors C. D. Anderson and E. W. Cowan both for their suggestions in determining the scope and purpose of the effort and their fruitful discussions which helped in carrying it to completion. The author is particularly indebted to their patience and encouragement which were of great benefit.

Most of the data included was obtained from the 5' x 5' cloud chamber designed by Professor E. W. Cowan and built by the cosmic-ray group. It was the availability of the data from this cloud chamber which made the project possible and the author would like to express his appreciation to Professor Cowan who supervised the construction and operation of the apparatus, to Messrs. Bruce Dean, Robert Lutermoser and Keith Mathews who helped with its construction and operation and the many other individuals involved with the project.

The author would also like to express his appreciation to the International Business Machines Corporation for the award of their fellowship and the California Institute of Technology and Office of Naval Research for their continued financial assistance.

ABSTRACT

An experiment to measure the inelastic scattering cross-section for nucleons with energies greater than 50 BEV on Iron has been carried out using a large multiplate cloud chamber as the detector and the cosmic-ray flux at Pasadena as the source of nucleons. This cross-section has been found to be $0.56 \pm .07$ barns and the corresponding nucleon-nucleon cross-section (averaged over protons and neutrons) to be 18 ± 5 mb. The average energy of the events included in the measurement is estimated at 250 BEV. These results have been compared with the inelastic scattering cross-section data available for energies above the π meson threshold.

An analysis has been made of the angular distribution of N-rays having energy greater than 50 BEV to determine the absorption mean free path in the atmosphere. Also it is shown that the neutral to charged particle ratio at a known depth in the atmosphere and the ratio of the mean free path for absorption to the mean free path for interaction are related to the average elasticity in nucleon-nucleon collisions, the former setting a lower limit and the latter, an upper limit. The absorption mean free path in the atmosphere is found to be 115 ± 15 gm/cm^2 and the elasticity is estimated at $(0.27 \pm .06) \leq \mathcal{E} \leq 0.45$.

TABLE OF CONTENTS

LIST OF FIGURES

I. INTRODUCTION

In order to test any model for nucleon-nucleon interactions it is necessary to predict some quantities which characterize that model and to experimentally determine the significance of these predictions. Hence it becomes important to accumulate as much experimental information as possible on any quantities which can aid in the development of a model and enable one to test it. Some of the quantities which, at the present time, appear significant are the angular distribution of the secondaries, the energy and momentum distribution among the secondaries, the cross-sections for production of different classes of secondaries, the multiplicity of the secondaries, etc. Since these quantities are, in all likelihood, energy dependent, it is necessary to carry out the measurements at a wide variety of energies. It was the purpose of this experiment to measure the cross-section for inelastic scattering and to make some estimate of the average elasticity of nucleon-nucleon interactions in the atmosphere.

A great deal of experimental work has been performed to determine the energy dependence of nucleon-nucleon cross-sections for energies between the meson threshold (~300 MEV) and 5 BEV (from the Bevatron). In addition some work has been carried out at higher energies using the proton beam from the CERN accelerator at an energy of ~25 BEV. Because of the rapid change of cross-section with energy below 1 BEV and the limited region of greater energy that has been investigated, it is difficult to extrapolate the cross-section energy relationship to high energies.

At present cosmic rays provide the only source of nucleons with energies above 25 BEV and have been used in a counter experiment to determine the cross-section for multiple particle production at 50 BEV. The availability of the large 5' x 5' multiplate cloud chamber has provided a means of detecting interactions of the penetrating component of cosmic rays in iron and hence to determine the inelastic scattering cross-section at an energy which represents the average energy of the incident flux greater than 50 BEV.

Unfortunately one cannot separate the protons from the π-mesons in the incident flux and hence the cross-section determined is actually an average over the total composition of the penetrating component of the cosmic rays excluding μ-mesons. Also because events can only be recognized if in the interaction, an energy of 50 BEV or more is transferred to the secondaries in such a fashion that it can be recognized, i.e., one particle does not carry off an extremely large proportion of the energy, the cross-section measured is for highly inelastic collisions.

The method used for this measurement was to determine the range of incident particles in the chamber for interactions in which an energy of 50 BEV or greater is transferred to secondary particles. The mean free path for such interactions is then calculated by appropriate statistical analysis taking into account that only a finite distribution of ranges is possible due to the size of the chamber, i.e., ranges greater than some maximum value called the gate length cannot be observed.

For those particles which do interact within the chamber it is possible to determine the charge of the incident particles and their angular distribution. Assuming that the flux of primary particles at the top of the atmosphere is isotropic and that the direction of high energy secondaries (greater than 50 BEV) created in the atmosphere is very nearly the same as the primary particle, an analysis of the angular distribution of the flux observed yields an estimate of the absorption cross-section of nucleons in the atmosphere.

An estimate of the average elasticity of nucleon-nucleon interactions, i.e., the ratio of the kinetic energy imparted to the incident and target nucleon after collision to their kinetic energy before collision, can be made by observing the ratio of neutrons to charged flux, and the ratio of the absorption thickness in air as measured from the angular distribution data to the interaction thickness as calculated from the inelastic cross-section measurement.

This estimate can be calculated by considering the relation between the number of secondaries which will be included (the criteria for the inclusion of a particle is that it have an energy greater than 50 BEV) and the elasticity of the interaction. For example if the elasticity were near zero, few of the secondary nucleons would be included and hence few neutral particles would be observed. On the other hand, if the elasticity were very near one, the secondaries would possess significant energy and be capable of in turn producing secondaries which might also be included and hence the ratio of neutrons to protons would be more

nearly one. Note that this does not mean that the ratio of neutrons to charged particles will also be near one. Also if the secondaries from the first interaction have enough energy to interact repeatedly, each yielding secondary nucleons which could be observed, a significant difference between the absorption and interaction mean free paths would be observed.

II. DESCRIPTION OF THE APPARATUS

The data discussed in this portion of the thesis was obtained with the 5' x 5' cloud chamber which has been in operation in the Cosmic Ray Laboratory since November 1958. This equipment, designed by Professor E. W. Cowan and shown schematically in Figs. 1 and 2, consists of a multiplate cloud chamber 150 cm high x 150 cm wide with a visible region approximately 60 cm deep, containing 11 iron plates averaging 2.93 cm thick. The density of the plates is 7.91 gm/cc; the total amount of material in the chamber is 254 gm/cm^2.

The expansions were triggered by two trays of G. M. tubes mounted below the chamber. Each array consisted of 8 counters and a total cross-sectional area of 4×10^3 cm^2. A coincidence of three counters in each of the two arrays was required for triggering. This coincidence was not strictly maintained since the coincidence requirement was made by adjusting the bias on a pulse height discriminator and the pulse heights from the counters was subject to some variation. For a short period of time, an additional coincidence was required from one counter in each of 3 out of 4 additional arrays, each array consisting of 8 counters. These four trays were mounted in the ceiling of the laboratory housing the cloud chamber at the corners of a square 15' on a side, one corner of the square being located directly above the chamber.

The photographs were taken by two cameras on 70 mm Linagraph Pan film, each camera using a single Ektanon 10-in. lens. The cameras are separated by 94 cm and mounted at a distance of

665 cm from the center of the chamber to the lens. An example of the photography is shown in Fig. 3.

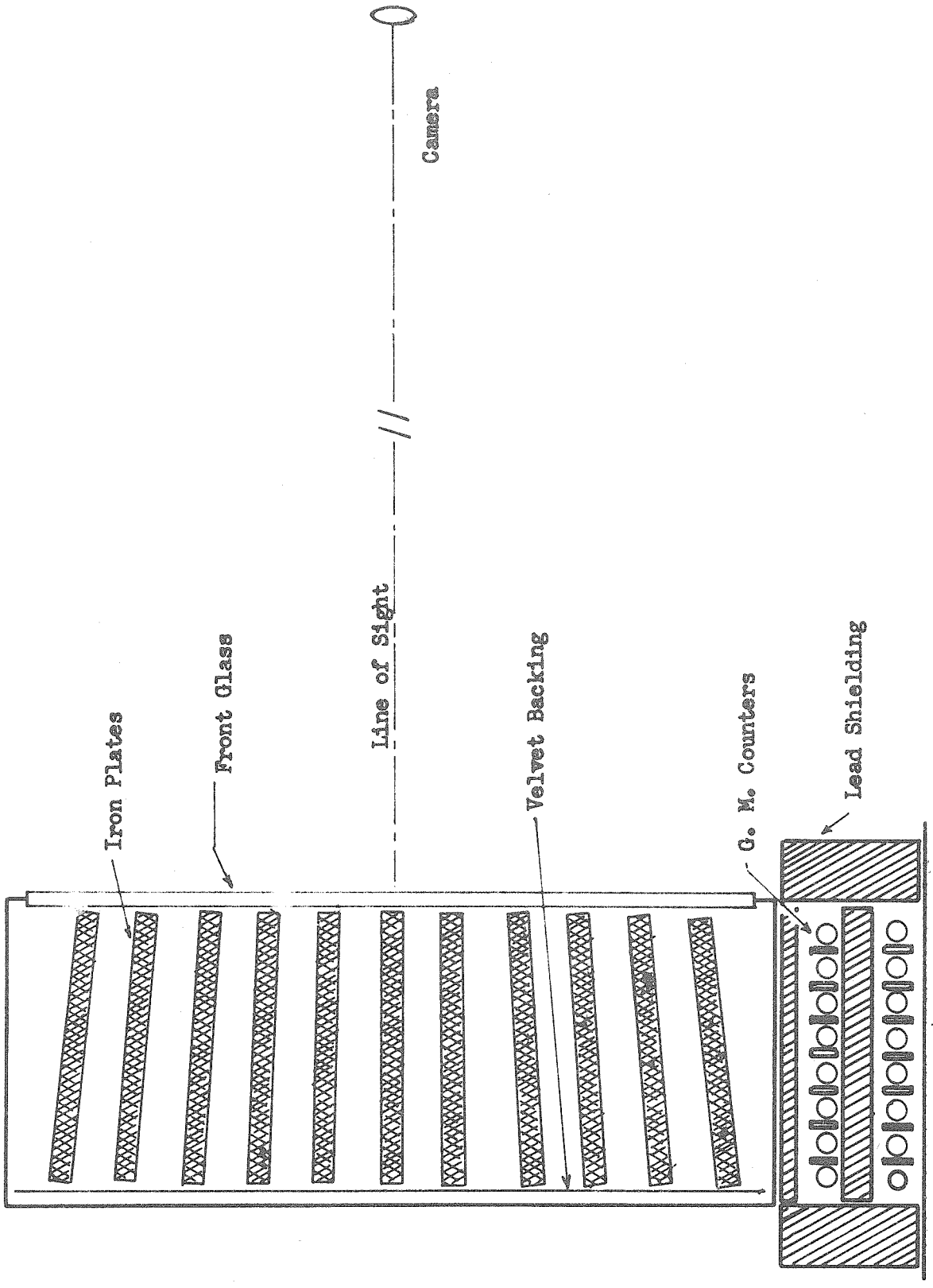

Fig. 1. 5' X 5' Cloud Chamber Profile

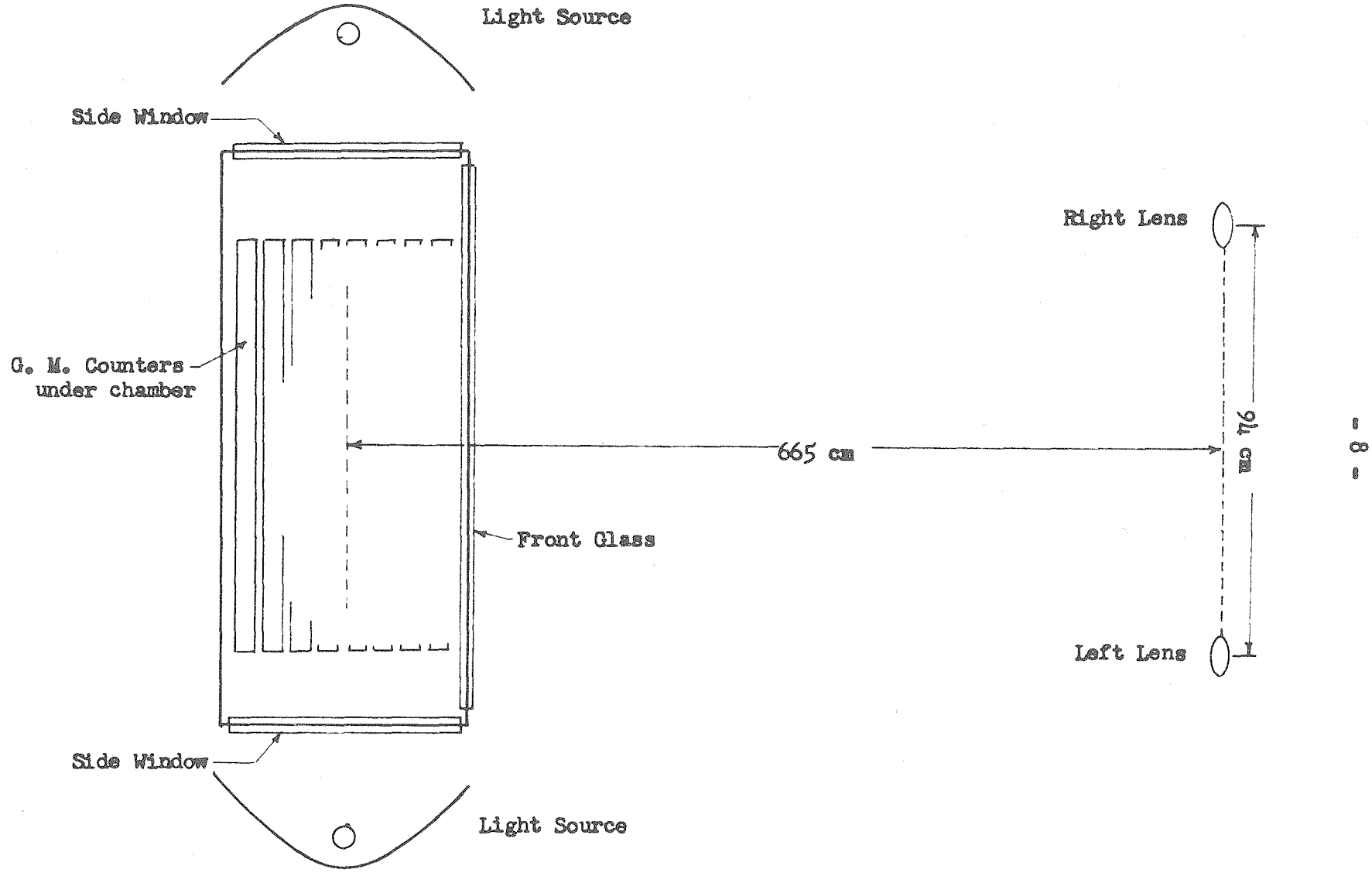

Fig. 2 5' X 5' Cloud Chamber Plan View

Fig. 3. Photograph taken with 5' X 5' Cloud Chamber. Charged primary interacting in third plate with a minimum energy of 500 BEV transferred to secondaries.

III. TABULATION OF DATA

A. Criteria for Selection of Events

A total of over 33,000 photographs were visually scanned using a stereoscopic viewer constructed for this purpose. From these photographs certain events were selected to be tabulated for the cross-section measurements according to the following criteria:

1. An interaction takes place below plate 1 and above plate 10 in which the energy of the primary particle can be estimated at 50 BEV or greater.
2. The projected line of flight of the primary crosses plates 1 and 11 in the visible region of the chamber.
3. Some particles heavier than electrons can be identified among the secondaries of the interaction.

The requirement that the interaction take place below plate 1 removes a large percentage of electron showers resulting from γ's produced above the chamber. Although criteria 3 also removes these events, the number of unwanted cases which must be observed in detail is greatly reduced by criteria 1. Also, since it is necessary to observe the secondaries from an interaction as they pass through a plate in order to estimate the energy, the requirement that the interaction take place above plate 10 (in effect in plate 9 or above) allows all tabulated events to be observed at least in the space between plates 9 and 10, 10 and 11, and 11 and the bottom of the chamber. This allows enough volume to be able to estimate whether the energy of the primary was above 50 BEV. It is impossible, of course, to determine how much more energy the primary

possessed since only a small portion of the shower is observed.

The probability of an interaction taking place within the volume of the chamber will depend, among other things, upon the mean free path for the particular type of interaction and the total thickness of material in the chamber. For the cosmic ray beam this thickness would be a function of the angle of incidence of the primary particles. This variation results both from the lengthening of the path through the iron plates due to the non-verticality of the beam and from the possibility of the line of flight passing through the walls of the chamber and avoiding some of the plates altogether. Criteria 2 eliminates the latter possibility and establishes a near constant gate length, the only variation being the small correction due to the lengthening of the path.

The type of interactions which one wishes to observe are those resulting from nucleon-nucleon collisions. Since it is impossible to distinguish between π mesons and nucleons and since the target consists of many nucleon-nuclei, one must be content with observing interactions between incident mesons and nucleons and the target nucleus, although it is usual to assume that at high energies the incident particle interacts with a single particle within the nucleus. For the measurement of cross-sections it is immaterial whether or not the secondaries from the interaction between the primary particle and the single nucleon proceed to interact with the remaining particles in the nucleus. Criteria 3 eliminates those events which result from electromagnetic interactions alone.

By these criteria, a total of 606 events were tabulated and the appropriate measurements made to determine range and energy.

In addition to the normal type of events which one would expect to find in high energy interactions, namely many secondaries in a narrow cone and additional secondaries in a wider cone, several events were noticed where a single secondary particle, usually emitted within 1 or 2 degrees of the line of flight of the primary, contained a major share of the energy, the remaining secondaries being few in number and emitted at large angles (in some events greater than 90^{o} in the lab system) and containing a relatively small share of the primary energy. Such an event is characterized by a primary interaction involving few particles and a secondary interaction involving many particles. The energy of the higher energy secondary can be estimated by observing its interaction lower in the cloud chamber. Both neutral and charged secondaries were observed and from preliminary examination of the neutrals, it appeared that the mean free path for these particles might be significantly less than for nucleons, but greater than would be expected for γ-rays, indicating that perhaps these might be some unstable particles such as Λ^{o}'s. Hence these events were tabulated according to the following criteria:

1. A secondary interaction can be recognized as the result of a single particle whose line of flight intersects the point of a primary interaction. (Charged secondaries must visibly originate from the primary interaction point.)
2. The secondary interaction must contain at least approximately 2/3 of the total energy of the primary particle.

No requirement was made on the line of flight of the primary or higher energy secondary, since, as the first interaction takes

place at varying depths in the chamber, each higher energy secondary would have a different gate length in any case. Also no discrimination was made against events which represented pure electron showers as a result of the secondary interactions since, for the neutral particles, at least two possibilities could be gamma rays resulting from π^{o}'s from the original interaction or from $\Lambda^{o} \rightarrow n + \pi^{o}$.

By these criteria a total of 40 events were tabulated and the appropriate measurements made to determine the range and energy of the primary and of the higher energy secondary.

B. Estimate of the Primary Particle Energy

A direct measurement of the energy of the primary particle is impossible; the only observation which can be made is the charge as observed by the track above plates 1 and 2. It is possible to sum the estimated energies of the secondaries as determined by multiple scattering and range measurements for the penetrating secondaries and the energy found in electron-photon cascades associated with the event[1]. Since neutral particles may escape detection entirely and a large number of charged particles in the forward cone may be indistinguishable, such a "calorimetric" method will only establish a lower limit to the energy. The degree of underestimate of the primary energy is difficult to calculate; however the percentage of the underestimate will be greater for higher energies, since at the higher energies the density of secondaries is much greater with a resulting increase in the relative number of them obscured by electron-photon cascades, by lack of resolution, and by saturation of the chamber. The purpose of estimating the energy was to select only those

events which were the result of primaries with energy greater than 50 BEV, hence the result of an underestimate is to shift the average energy of the tabulated events upwards rather than to include lower energy interactions.

Another type of estimate may be made based upon the kinematics of the interaction[1-9]. This method requires the assumption of a model for the fundamental process and some additional assumptions. One assumes that the event is due to a collision of a particle of mass m with a single target nucleon of mass M, that the secondaries are emitted with relativistic velocities, and also that the secondaries are isotropically distributed in the center of mass system. On this basis, a relation between the half angle $\theta_o/2$ of the forward cone of the secondaries and the energy E_p of the primary particle can be derived. (See Appendix I). This calculation results in the so-called median angle formula:

$$E_p = \frac{2Mc^2}{(\tan\frac{\theta_o}{2})^2} \qquad (1)$$

If the primary particle is identical to the target nucleon then the assumption that there is symmetry in the center of mass system about a plane perpendicular to the line of flight and that the forward cone will contain half of the secondaries is valid. However, Eq. 1 in general will yield an overestimate of the energy since it is based upon the assumption that the particles defining the inner cone are emitted at an angle of 90^o in the center of mass system whereas, in actual fact, they will be emitted at a smaller

angle.

The estimate of the primary energy is made by setting as a lower limit the estimated energy transferred to the secondaries and for higher energy events evaluating the energy from the opening angle of the forward cone and using a subjective judgement to arrive at a final estimate.

C. Measurement of the Range of the Primary

The point of interaction within a plate of the cloud chamber was located by projecting the trajectory of several secondaries back through the plate and estimating the fraction of plate thickness which was traversed by the incident particle. For charged primaries this could be further checked by extending the line of flight of the primary forward. In all cases several secondaries were included to determine the interaction point and it is estimated that this measurement is accurate to 20% of a plate thickness.

By adding the number of plates traversed, excluding plate 1, to the fraction of plate included to the point of interaction, the range, in terms of plate thickness, was determined. Because of the large solid angle subtended by the cloud chamber it was necessary to make an angular correction to find the true thickness of iron penetrated. The angle θ between the trajectory and vertical was measured in the left and right views, θ_L and θ_R respectively, and by the analysis of Appendix B, sec θ was determined to be:

$$\sec\theta = \sqrt{1 + \left[\frac{1}{2}(\tan\theta_L + \tan\theta_R)\right]^2 + \left[\frac{d}{2s}(\tan\theta_L - \tan\theta_R)\right]^2} \qquad (2)$$

The errors in range measurement result from inaccuracy in determining the interaction point, errors in measuring θ_L and θ_R, and from the approximation in Eq. 2. For particles which traverse many plates, the major error is in the angular correction which has a maximum value of approximately 7%. If the interaction occurs in the first few plates, the largest error will result from the indeterminacy of the interaction point. In either case, these errors are equally likely to shorten or lengthen the range measured and hence will have a small effect when averaged over all events.

The tilting of the plates was not taken into account in any of the measurements, hence additional errors will be present. The maximum error presented by this effect is less than 1/2% and is entirely negligible compared to the large statistical errors inherent in the experiment.

IV. PROCEDURE FOR CROSS-SECTION MEASUREMENT

A. Method of Maximum Likelihood

The application of maximum likelihood procedure to the measurement of the lifetimes of unstable particles has been discussed by many authors[10-13] using both cloud chamber and photoemulsion data. This procedure is easily extended to the measurement of the range of a high energy particle.

Let P(x) be the probability that a particle has traversed a thickness x of material, measured from some established reference plane. The probability dp(x) that the particle interacts at x in an interval dx is given by:

$$dp(x) = \lambda P(x)dx \tag{3a}$$

Since $dp(x) = -dP(x)$, Eq. 3a may be integrated to solve for P(x) yielding:

$$dp(x) = \lambda C e^{-\lambda x} dx \tag{3b}$$

By the discussion of section III-A, namely that only particles which interact in some maximum distance L_g, the gate length, are included, the total probability that the particle will interact in $0 \leq x \leq L_g$ is 1. Hence

$$\int_0^1 dp(x) = \int_0^{L_g} \lambda C e^{-\lambda x} dx = C(1-e^{-\lambda L_g}) = 1$$

and

$$dp(x) = \frac{\lambda e^{-\lambda x}}{1 - e^{-\lambda x}}\, dx \tag{3c}$$

The quantity λ is the reciprocal of the mean free path, L_c, where L_c is defined as the thickness of material required to reduce the probability of interaction to 1/e for infinite gate length.

Thus the probability of a single particle having a range x_i within an interval Δx for a gate length L_i is represented by:

$$p_i = \frac{e^{-x_i/L_c}}{L_c(1 - e^{-L_i/L_c})} \Delta x \tag{4}$$

and the probability of obtaining a particular set of experimental data from a sample of N independent events is[14]:

$$P = \frac{(N-1)!}{\prod(N_i!)} \prod_{i=1}^{s} \{\frac{e^{-x_i/L_c}}{L_c(1-e^{-L_i/L_c})} \Delta x\}^{N_i} \tag{5}$$

where N_i is the number of events having range x_i within an interval x_i and s is the number of distinct values of x_i*.

The method of maximum likelihood consists simply of choosing the value of the parameter which makes P a maximum. Since in this expression the parameter is only included in the function in the brackets, one wishes to find the value of L_c for which

$$\prod_{i=1}^{N} \{\frac{e^{-x_i/L_c}}{L_c(1-e^{-L_i/L_c})}\}$$

is a maximum.

Defining

$$\mathcal{L} = \sum_{i=1}^{N} \ln (\frac{e^{-x_i/L_c}}{L_c(1-e^{-L_i/L_c})}) \tag{6}$$

*For x_i sufficiently small, i.e. such that no two events have the same values of x_i, this reduces to:

$$P = (N-1)! \prod_{i=1}^{N} \frac{e^{-x_i/L_c}}{L_c(1-e^{-L_i/L_c})} \Delta x \tag{5a}$$

the most likely value of L_c is given by

$$\frac{\partial \mathcal{L}}{\partial L_c} = 0 \tag{7}$$

and the standard deviation of L_c by a second differentiation from the formula

$$\frac{\partial^2 \mathcal{L}}{\partial L_c^2} = -\frac{1}{\sigma^2} \tag{8}$$

the latter expression being applicable only where L_c is normally distributed as is often the case with considerable accuracy in large samples. Carrying out the differentiation indicated in Eqs. 7 and 8

$$L_c = \frac{1}{N} \sum_{i=1}^{N} \left\{ x_i - \frac{L_i}{e^{L_i/L_c} - 1} \right\} \tag{9}$$

$$\sigma = L_c \left[\sum_{i=1}^{N} \left\{ 1 - \frac{L_i^2}{L_c^2} \frac{e^{L_i/L_c}}{(e^{L_i/L_c} - 1)^2} \right\} \right]^{-\frac{1}{2}} \tag{10}$$

Given a set of x_i and L_i from the data obtained in the cloud chamber experiment, Eq. 9 can be solved by iteration to find the most probable value of L_c.

In the particular case where the gate length is constant for all of a class of events, i.e. all $L_i = L_g$, Eqs. 9 and 10 reduce to:

$$L_c = \frac{1}{N} \sum_{i=1}^{N} x_i - \frac{L_g}{e^{L_g/L_c} - 1} \tag{11}$$

$$\sigma = L_c \left[N \left\{ 1 - \frac{L_g^2}{L_c^2} \frac{e^{L_g/L_c}}{(e^{L_g/L_c} - 1)^2} \right\} \right]^{-\frac{1}{2}} \tag{12}$$

The solution to Eqs. 11 and 12 is shown graphically in Fig. 4.

The standard deviation σ is a measure of the error under the a priori assumption that Eq. 3 adequately represents the probability that an interaction takes place at x_i in the interval dx which in turn assumes that for all events a unique value of L_c exists. If the incident flux is composed of two components having different cross-sections, the value of L_c obtained by this procedure will be some average which represents the best fit which can be made between the single exponential curve and the double exponential curve which actually exists. The standard deviation calculated in this case will have very little meaning.

The maximum likelihood calculations appear to be dependent only upon the average range of all events and do not make use of the information available regarding the distribution of ranges. However Fisher[10] has pointed out that this procedure satisfies the criteria of sufficiency and makes maximum use of the available information. Also the value of σ obtained with Eq. 10 is the least possible value for the standard deviation designed to estimate the parameter and may therefore be applied to calculate the efficiency of any other statistic. That no additional information is gained from consideration of the distribution of the interactions beyond the determination of the average range follows from the a priori assumption of Eq. 3 and hence the assumed relationship between the distribution and the average value, the only difference resulting from the statistical fluctuations included in σ. Before applying this method, therefore, the validity of Eq. 3 must be tested. This can be done by comparing the distribution of ranges with that predicted under the assumptions of Eq. 3.

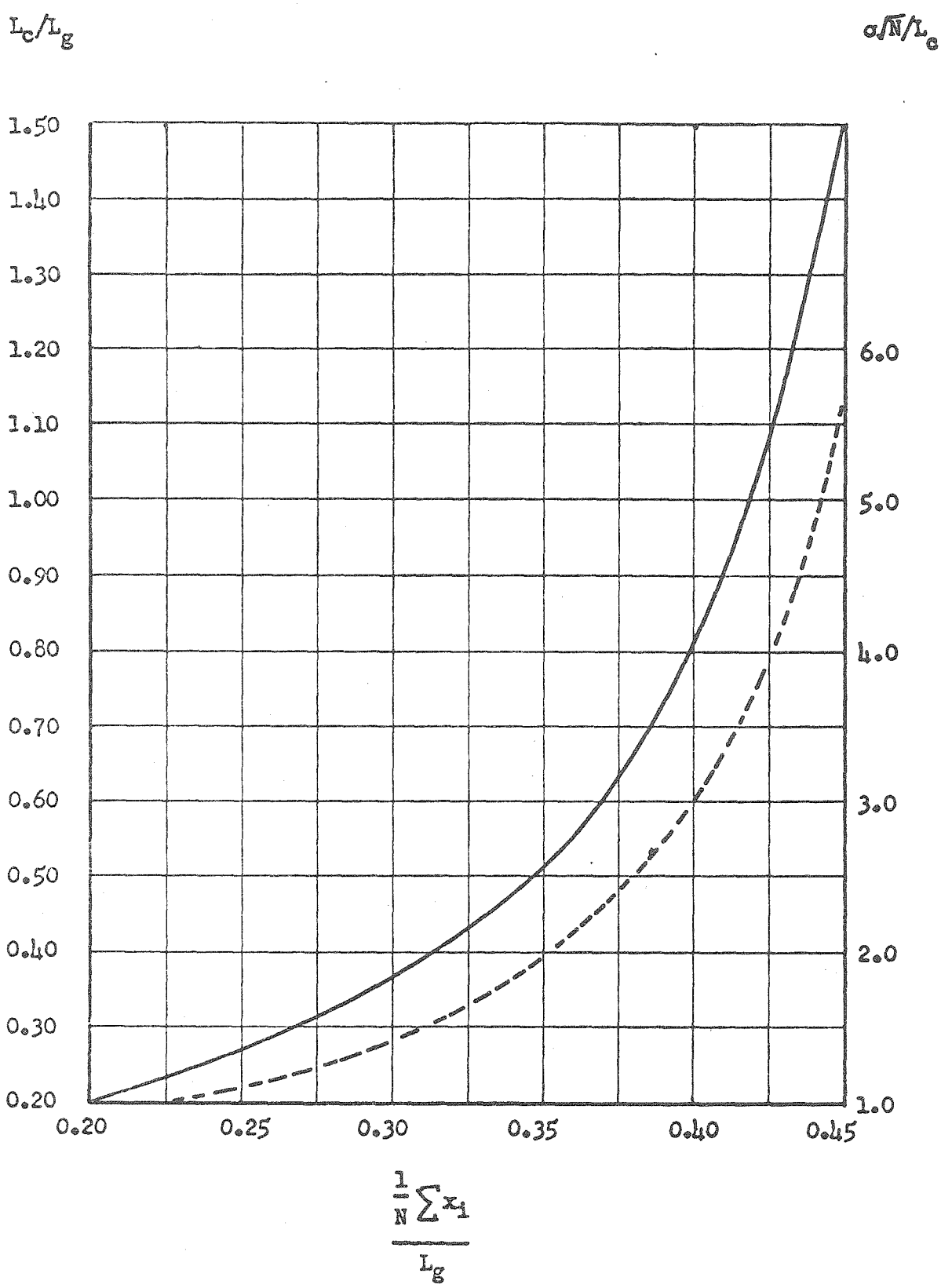

Fig. 4. Solution to Eqs. 11 and 12 in terms of normalized coordinate $\langle x_i \rangle / L_g$. Solid curve represents L_c/L_g, dashed curve represents $\sigma\sqrt{N}/L_c$.

B. Distribution of Ranges for Constant Gate-Length

The method described here is based on an analysis of the distribution of ranges of the interacting particles assuming Eq. 4 is valid and the gate length for all events is constant. Let:

L_g = gate length for all events.

L_c = mean free path of the incident particles.

$N_o(x)$ = the number of primaries at a distance x from the fiducial line which are observed to interact in allowed gate length.

$N_t(x)$ = the true number of primary particles at a distance x from the fiducial line.

N_f = the number of primary particles which go unobserved, i.e., do not suffer inelastic collisions in L_g.

Then:

$$N_t(x) = N_o(x) + N_f \tag{13}$$

The number of interactions, dN, observed at a distance x in an interval dx follows from Eq. 3 as

$$dN = \frac{1}{L_c} N_t(x)dx \tag{14}$$

Since $dN/dx = - dN_t(x)/dx$, Eq. 14 may be integrated to

$$N_t(x) = N_t(0)e^{-x/L_c} \tag{15}$$

By the definition of N_f

$$N_f = N_t(L_g) = N_t(0)e^{-L_g/L_c} \tag{16}$$

Hence the equivalent of Eq. 3 in terms of the numbers of events is

$$N_t(x) = \frac{N_o(0)e^{-x/L_c}}{1-e^{L_g/L_c}} \tag{17}$$

yielding for the number of interactions, n_i, observed in the interval Δx centered about the distance x_i

$$n_i = \frac{N_o(0)\, e^{-x_i/L_c}}{L_c(1-e^{-L_g/L_c})}\, \Delta x \tag{18}$$

This may be put in a more convenient form by taking the natural logarithm

$$\ln(n_i) = \ln \frac{\Delta x\, N_o(0)}{L_c(1-e^{L_g/L_c})} - \frac{x_i}{L_c} \tag{19}$$

The values of $N_o(0)$, L_c and L_g are assumed to be constants for any set of data and Δx may be chosen to have a fixed value. Hence Eq. 19 has the forms of the straight line

$$y_i = ax_i + b \tag{20a}$$

where $y_i = \ln(n_i)$

$$a = -\frac{1}{L_c} \qquad b = \ln \frac{\Delta x\, N_o(0)}{L_c(1-e^{L_g/L_c})} \tag{20b}$$

For a given set of data, (x_i, y_i), the best estimate of a and b, α and β respectively, may be obtained by making a least square fit between the data and Eq. 20[15, 16], weighting each set of points proportionately to the inverse of the variance of y_i. This yields as the estimates of a and b

$$\alpha = \sum_{i=1}^{n} \left[\left(\frac{A}{D} x_i - \frac{B}{D} \right) w_i y_i \right] \tag{21a}$$

$$\beta = \sum_{i=1}^{n} \left[\left(\frac{C}{D} - \frac{B}{D} x_i \right) w_i y_i \right] \tag{21b}$$

where $A = \Sigma w_i$ $\quad C = \Sigma w_i x_i^2$

$B = \Sigma w_i x_i$ $\quad D = AC - B^2$

and as the variances in α and β.*

$$\sigma_\alpha = \sigma_y \Sigma \left[w_i \left(\frac{A}{D} x_i - \frac{B}{D} \right) \right]^2 \tag{22a}$$

$$\sigma_\beta = \sigma y \Sigma \left[w_i \left(\frac{C}{D} - \frac{B}{D} x_i \right) \right]^2 \tag{22b}$$

where $$\sigma_y = \frac{\Sigma [w_i (y_i - \alpha x_i - \beta)^2]}{\Sigma w_i (n-2)}$$

C. Calculation of Cross-section per Nucleon from Mean Free Path Determination

Defining the mean free path, L_c, as the thickness of material required to reduce the probability that the particle has not interacted to 1/e and assuming that each nucleus represents an obstacle with cross-sectional area $\sigma_{nuc.}$, one can derive the following relationship:

$$\sigma_{nuc.} = \frac{A}{NL_c} \tag{23}$$

where A is the atomic mass number, N is Avogadro's number and L_c is the mean free path expressed in gm/cm^2. $\sigma_{nuc.}$ will represent the nuclear cross-section for the process for which the mean free path is L_c. In this experiment, the cross-section determined will be the cross-section for inelastic scattering, or more appropriately, the cross-section for multiple particle production.

*Worthington and Geffner (Ref. 15) err in their derivation of these quantities, however the correct expression follows directly from their reasoning.

In order to compare the results of this experiment with that of other workers, it is necessary to determine the cross-section per nucleon rather than per nucleus since the target materials vary from experiment to experiment and also since the fundamental process of interest is nucleon-nucleon interactions.

If one assumes that the mean free path of nucleons through nuclear material is large compared to nuclear dimensions and that for high energy events, the nucleons in a nucleus can be considered to be independent, the relationship between the elementary cross-section and the nuclear cross-section is

$$\bar{\sigma} = \frac{\sigma_{nuc.}}{A} \tag{24}$$

where $\bar{\sigma}$ is the cross-section per nucleon averaged over both protons and neutrons for measurable events. This would represent an extreme value for a highly transparent nucleus.

The inelastic cross-section for iron as a function of $\bar{\sigma}$ has been calculated by Brenner and Williams[18] and Alexander and Yekutreli[19] based upon the optical model of Fernbach, Serber and Tayler[20]. Brenner and Williams, using as the density distribution function, the charge distribution function, $\rho_e(r)$ measured by Hofstadter and his collaborators[21], adjusted the parameters of $\rho_r(r)$ to give the best fit to the cosmotron experiments at near 1 BEV for an effective elementary cross-section of 30 mb. Alexander and Yekutreli, using the charge distributions of Hofstadter[22, 23], Meyer-Berkhout et al.[24], and Helm[25] (the selection of each distribution was chosen to give best agreement with experimental data)

calculated the transparency curve for a series of nuclei and have extrapolated the curve for iron. These results agree within a few percent of those of Brenner and Williams which have been plotted in Fig. 5.

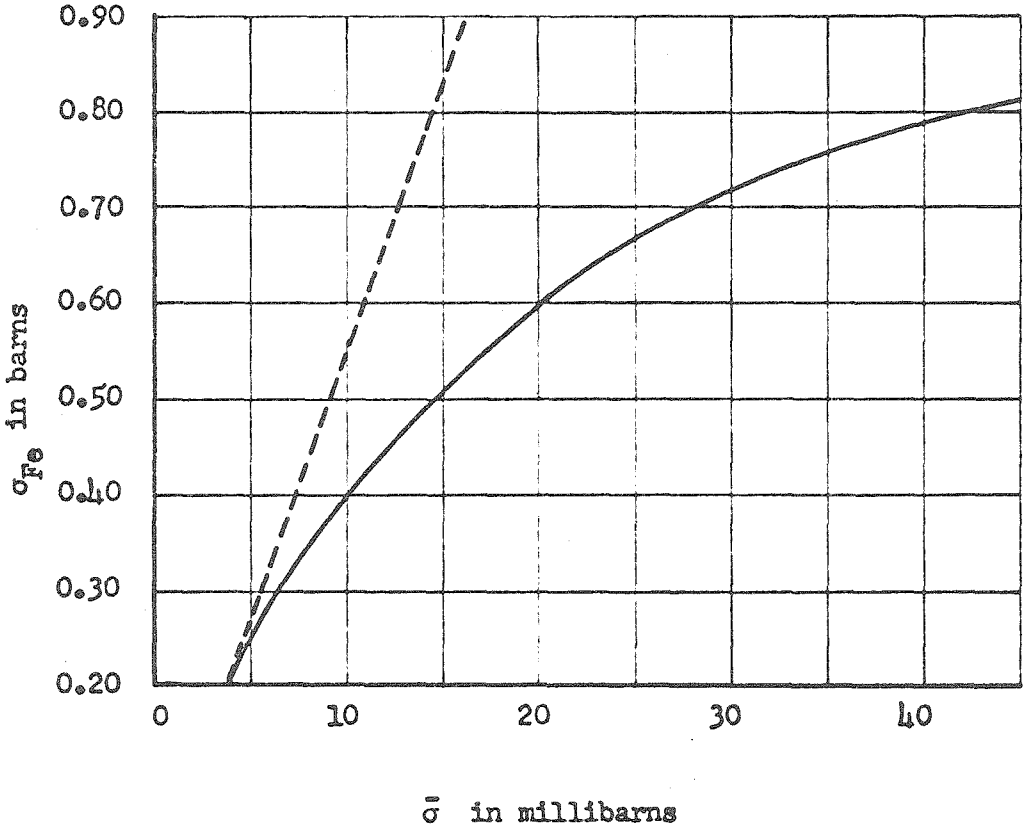

Fig. 5. Transparency curve for Fe, calculated by using the parameters of the effective density distribution $\rho_e(r)$: $t = 2.6 \times 10^{-13}$ cm and $r_1 = 1.15 \times 10^{-13}$ cm. The dashed curve represents $A\sigma$, the cross-section for a completely transparent nucleus. (After Brenner and Williams)

V. DISCUSSION OF THE DATA

A. Cross-Section for Multiple-Particle Production at Energies Above 50 BEV

A total of 606 interactions were selected according to the criteria outlined in sec. III-A. Of these 108 were the result of neutral primaries and 498 the result of charged primaries. The minimum energy included in the data was 50 BEV and the bias in selection was such as to underestimate the energy.

The gate-length for inclusion in the tabulation corresponded to 8 plate thicknesses or 185 gm/cm^2 for normally incident particles. The gate-length for inclusion in the calculation was thus taken as 185 gm/cm^2. Of the 606 tabulated events, 3 neutral and 10 charged primaries had ranges in excess of this value and were discarded leaving a total of 593 events, 105 neutral and 488 charged.

The mean free path in iron determined from maximum likelihood procedure along with the pertinent data is shown in Table I. The tolerance indicated is the standard deviation as calculated from Eq. 12, and does not include systematic or statistical errors other than those resulting from the counting statistics as calculated from the maximum likelihood procedure.

The validity of the assumptions for the maximum likelihood calculation can be checked by examination of the distribution of ranges as described in section IV-B. Table II gives the experimental data obtained which has been plotted in Figs. 6, 7, and 8. The values obtained for the mean free path from the data of Table II along with other pertinent results are given in Table III.

TABLE I

Data for Maximum Likelihood Calculation

	Neutrals	Charged	Total
Number of Events	105	488	593
L_g (gm/cm^2)	185	185	185
$\langle x_i \rangle$ (gm/cm^2)	74.0	75.9	75.5
$\langle x_i \rangle / L_g$	.400	.410	.408
L_c/L_g	.82	.91	.90
L_c (gm/cm^2)	152 $\pm$ 42	168 $\pm$ 25	167 $\pm$ 22

TABLE II

Number of interactions, n_i, observed with range, x_i, in interval $\Delta x = 20$ gm/cm^2.

x_i	Neutrals		Charged		Total	
(gm/cm^2)	n_i	$\ln(n_i)$	n_i	$\ln(n_i)$	n_i	$\ln(n_i)$
10	19	2.94	79	4.37	98	4.59
30	15	2.70	77	4.35	92	4.51
50	15	2.70	68	4.22	83	4.42
70	13	2.57	49	3.89	62	4.13
90	9	2.93	52	3.95	61	4.11
110	13	2.57	41	3.71	54	3.99
130	9	2.29	42	3.74	51	3.91
150	6	1.79	38	3.64	44	3.78
170	6	1.79	27	3.30	33	3.50

TABLE III

Data From Distribution of Ranges

	Neutrals	Charged	Total
α (cm^2/gm)	-6.3×10^{-3}	-6.2×10^{-3}	-6.2×10^{-3}
σ_α	7.4×10^{-4}	3.5×10^{-4}	3.0×10^{-4}
β	2.99	4.48	4.68
σ_β	3.3×10^{-2}	1.9×10^{-2}	1.8×10^{-2}
b (calculated)[1]	2.98	4.51	4.70
b (from Table I)[2]	2.97	4.47	4.65
L_c (gm/cm^2), $(-1/\alpha)$	160 ± 19	161 ± 9	161 ± 8

1. b (calculated) is the value of b obtained using Eq. 20b with the value of L_c obtained from the mean square fit.

2. b (from Table I) is the value of b obtained using Eq. 20b with the value of L_c obtained from the maximum likelihood procedure.

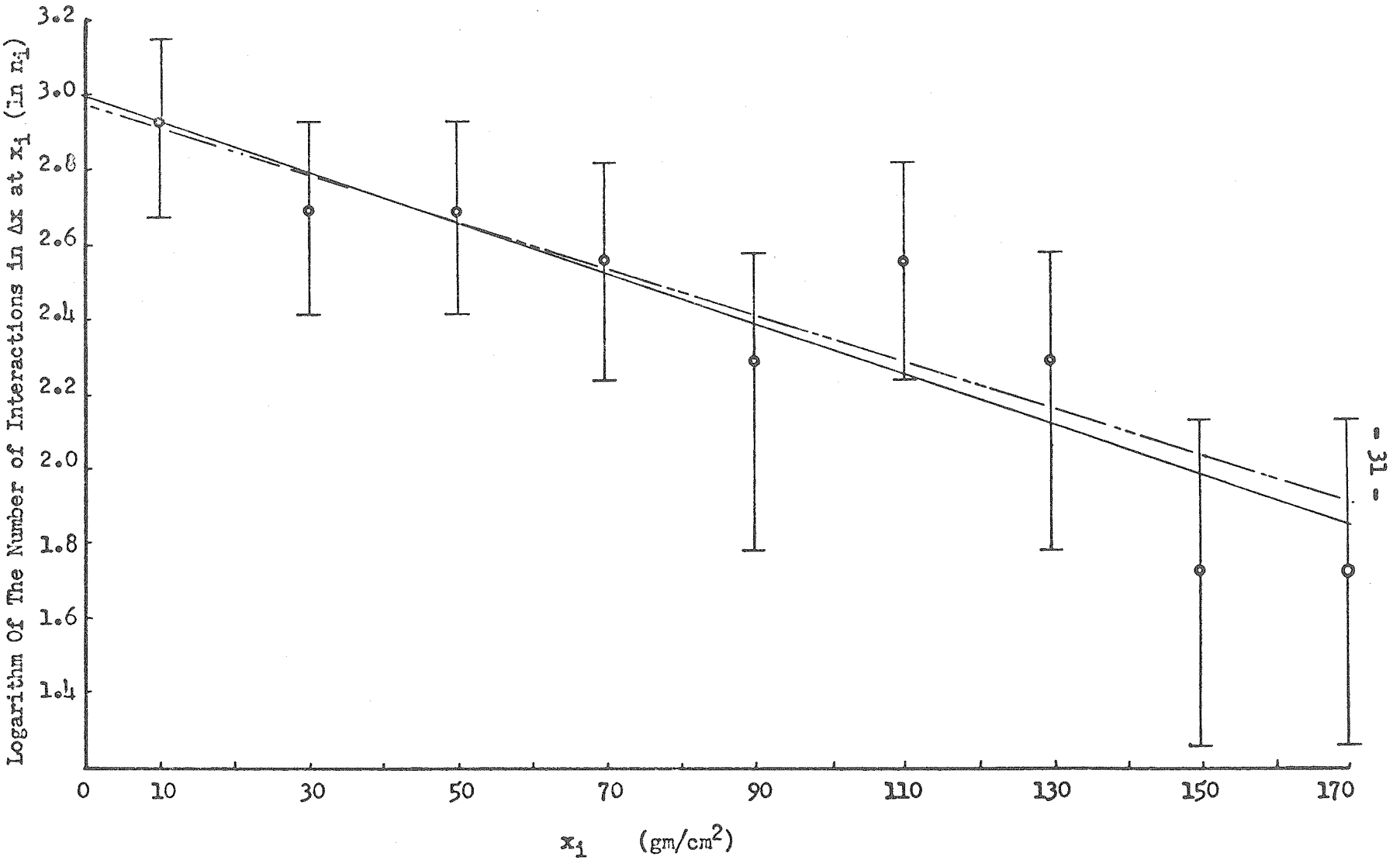

Fig. 6. Distribution of ranges for neutral events. $\Delta x = 20$ gm/cm^2. Broken curve is mean square fit to data, solid curve is maximum likelihood approximation.

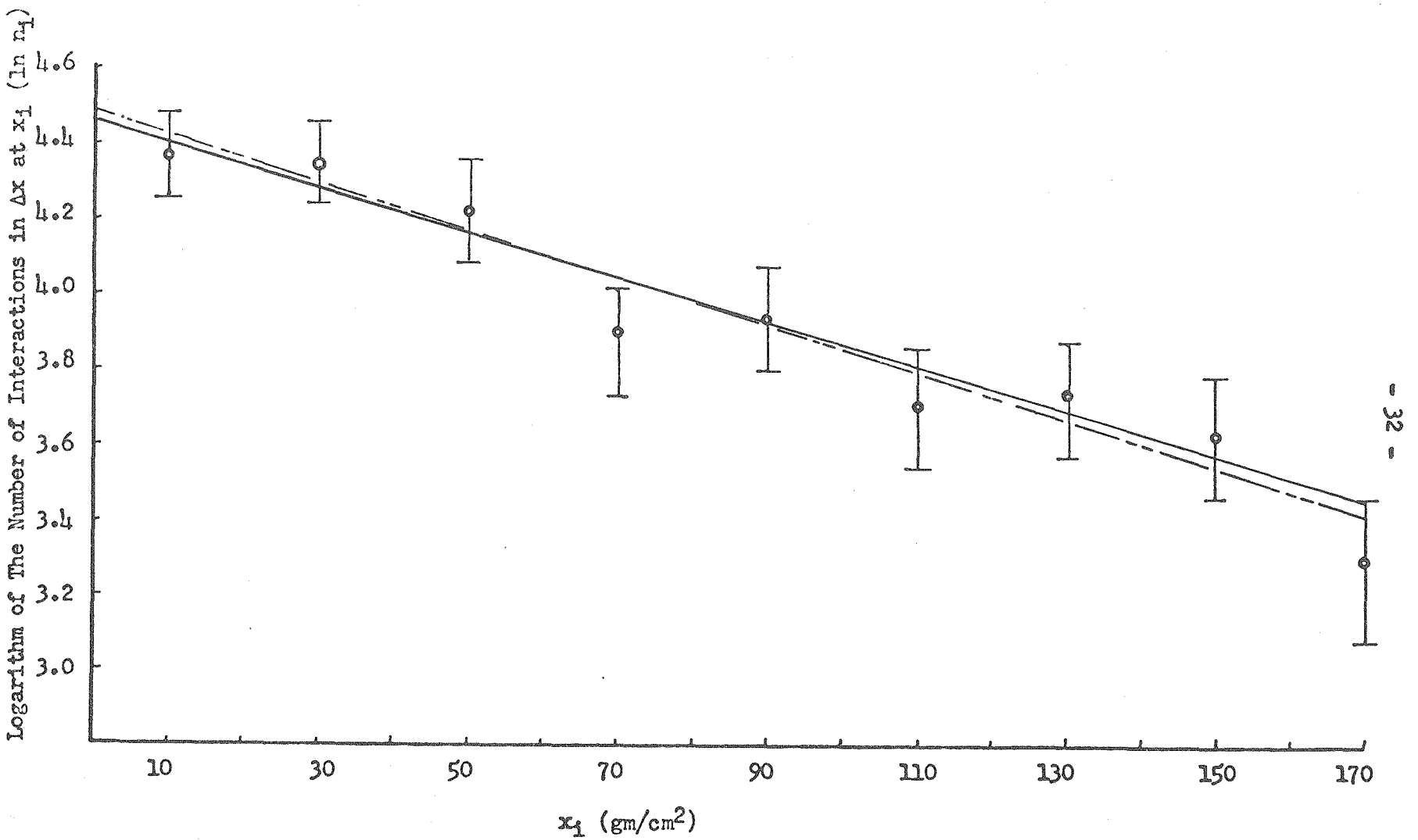

Fig. 7. Distribution of ranges for charged events. $\Delta x = 20$ gm/cm^2. Broken curve is mean square fit to data, solid curve is maximum likelihood approximation.

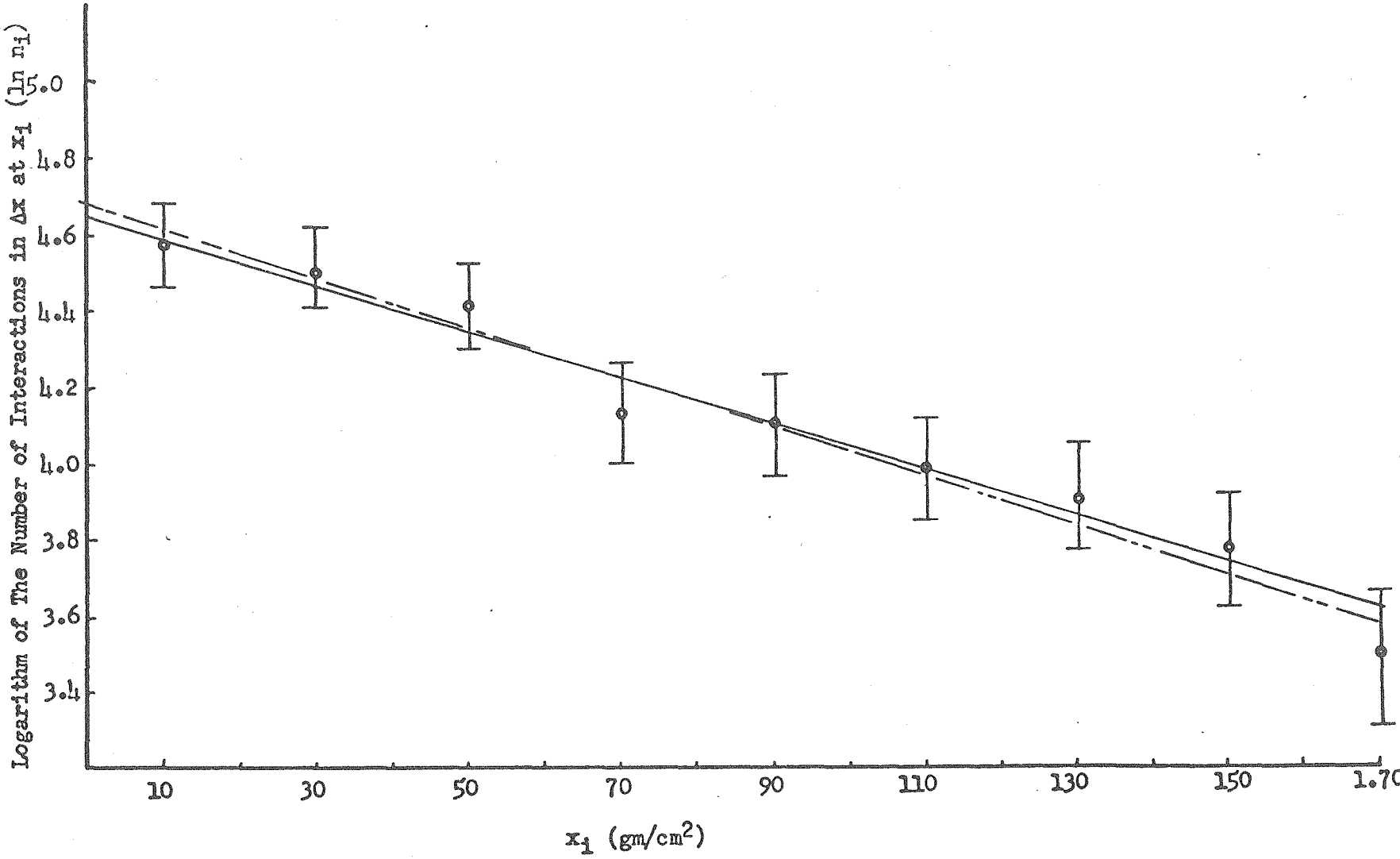

Fig. 8. Distribution of ranges for all events. $\Delta x = 20$ gm/cm^2. Broken curve is mean square fit to data, solid curve is maximum likelihood approximation.

From inspection of Figs. 6, 7 and 8 as well as the close agreement of the values of α and β in Table III and the values from the maximum likelihood calculation it appears that there is no inconsistency in the assumption of Eq. 4 and the data. The small standard deviations in α and β do not, however, indicate any increased accuracy in the determination of L_c over that obtained from the maximum likelihood calculation, only that the observed values of n_i lie very close to the evaluated line. In fact, as pointed out previously, the standard deviation as estimated by the maximum likelihood procedure is the most efficient statistic and may be used to estimate the efficiency of other statistics. The deviations included in Table III do not include the statistical uncertainty in each of the values of n_i.

Since the charged flux consists of both protons and π-mesons, the cross-section calculated for the charged events represents some average of the two. However, although the total cross-sections for π-mesons and protons have been shown to be significantly different at energies above a few BEV[26], the cross-section for inelastic scattering has been shown by Bowen et al. to agree within experimental error[27]. Also the close agreement between the data and the straight line of Fig. 8 as well as the consistency of the cross-section for neutral and charged primaries indicate that the result for charged primaries may be taken as the value for protons.

The errors in the determination of the mean free path arise from the following sources:

1. Statistical errors resulting from the random nature of the interactions.

2. Errors in the range measurement.

3. Biases in chamber operation and data reduction.

The first of these is accurately estimated by the maximum likelihood procedure and is determined by Eq. 12.

The error in range measurement is discussed in section III-C and can amount to 5 gm/cm^2 in the range of any particle. This error is normally distributed, hence the total error in the sum of the path length for n events will be $\sqrt{n}$ 5 gm/cm^2 and the error in the average path length will be $\frac{1}{\sqrt{n}}$ 5 gm/cm^2. For n = 500 with an average range of 75 gm/cm^2, this error will be .22 gm/cm^2. From the slope of the solution to Eq. 9 (Fig. 4) the error in $< x_i > / L_g$ results in an error 10 times as great in L_c/L_g yielding as the error in L_c, 2.2 gm/cm^2 or 1.4%.

The most serious errors, other than the statistical fluctuations, can arise from any bias in the reduction of the data or the operation of the chamber. Such a bias does exist in the estimate of the primary energy and must be considered when determining the average energy over which the cross-section is measured. Two additional biases which directly affect the range measurement are:

1. An increasing probability of identifying an event as having an energy of 50 BEV or greater for decreasing range.

2. A decreasing probability of triggering the chamber for decreasing range.

The first of these results from the increased ability to determine the energy of the primary as more of the shower is visible. By including only interactions which take place in plate 9 or before, and requiring only that an event have an energy of 50 BEV or greater,

this bias is minimized and at worst would show a decrease in the number of interactions nearer the end of the range.

The second bias would be in the opposite direction and results from the use of G.M. counters mounted below the chamber for triggering. The probability of secondaries from an interaction reaching the counter tray would be reduced for events which occur high in the chamber and hence have shorter ranges. This results both from the absorption of the secondaries in the remaining plates and the angular spread of the shower. For primaries with energies greater than 50 BEV, this effect will be small and at worst would decrease the number of interactions very near the beginning of the range. Because of the close agreement between the data and the assumptions of Eq. 4, both of these biases are considered small compared to the large statistical uncertainty of the determination.

The energy of the primaries obtained by averaging the values estimated for all events is approximately 150 BEV. However, as stated previously this is a severe underestimate of the energy since for many particles a value of 50 BEV was tabulated as the minimum observable energy. Assuming that there is no bias in the selection of events above 50 BEV dependent on energy, a better estimate of the average energy may be obtained by integrating the energy spectrum of the penetrating component of cosmic rays. This spectrum given by Peters[28] as:

$$dN \sim E^{-(s+1)}dE \text{ where } s = \begin{cases} 1.1 & \text{for } 10 \text{ BEV} \\ 1.48 & 10^3 \text{ BEV} \\ 1.78 & 10^6 \text{ BEV} \end{cases}$$

yields for the average energy of particles above 50 BEV, the value

of 230 BEV. In order to compensate for those events which have an energy above 50 BEV, but were not included due to the underestimate in energy, the average energy of the primaries is taken as 250 BEV.

The mean free path of nucleons in iron and the cross-section for multiple particle production (from Eq. 23) is therefore estimated as:

$$L_c = 167 \pm 22 \quad gm/cm^2$$
$$\sigma_{Fe} = .56 \pm .07 \text{ barns}$$

for nucleons with energies greater than 50 BEV.

From the transparency curve for iron (Fig. 5) this value of σ_{Fe} corresponds to an elementary cross-section for meson production of $\bar{\sigma} = 18 \pm 4$ mb. Since the Fe curve itself depends upon the assumed value of $\bar{\sigma}$ at 1 BEV, the error should include the uncertainty of $\bar{\sigma}$ at 1 BEV. Compounding this error with the statistical error, the value of $\bar{\sigma}$ for an average energy of 250 BEV is estimated to be

$$\bar{\sigma} = 18 \pm 5 \text{ mb}$$

B. Comparison with Other Data

Several determinations of the cross-section for inelastic scattering at higher energies for a variety of nuclei have been made using absorption techniques with high energy accelerators, cloud chambers used with an accelerator, cloud chambers with the cosmic ray flux and counter experiments with the cosmic ray flux. A summary of the results is given in Table IV and σ_{Fe} as a function of energy is plotted in Fig. 9. For the cases, as indicated in Table IV where the cross-section was not measured for iron, the value

plotted is an interpolation determined by plotting the cross-sections measured as a function of $A^{2/3}$. The value obtained from this experiment is also included.

From examination of Fig. 9, it is apparent that for energies above 1 BEV the inelastic scattering cross-section does not depend strongly upon energy. However one cannot conclude that the cross-section is constant at high energies as the data is equally reconcilable with a logarithmic decrement in cross-section as with a leveling off of cross-section at a value near .60 barns for energies above a few BEV.

It is interesting to note that the eight results obtained with a variety of methods and different incident particles lie very close to the straight line given by $\sigma_{Fe} = .72 - .07 \text{ Log } E$. Unfortunately, the large variance in each of the determinations of σ_{Fe} prohibits attaching any significance to this line.

A large number of experiments, especially at lower energies, have been performed to determine the nucleon-nucleon inelastic scattering cross-section. A summary of the results is given in Table V and $\overline{\sigma}$ as a function of energy is plotted in Fig. 10. The standard deviations have been included only for energies above 1 BEV for the sake of clarity. Again it is interesting to note the close correlation between the experimental values and the curve drawn through them. The only serious deviation from this curve occurs at 9 BEV and in this instance the data is very much in doubt. The actual value of σ quoted by Bogachev[45] was 21 mb. However this was obtained by subtracting the elastic from the total cross-section, and the value of the total cross-section given was inconsistent

with the results of Vivargent et al.[46] obtained with the large accelerator at CERN in a much superior experiment. Hence the value of Bogarchev was renormalized to fit the result of Vivargent et al. It is very likely that the value for the elastic scattering cross-section suffers in a similar fashion. In any case, from examination of Fig. 10, it is apparent that for energies above 1 BEV, the nucleon-nucleon scattering cross-section does not depend strongly upon energy, but one cannot conclude that the cross-section is constant at higher energies since the data is equally consistent with a logarithmic decrement in cross-section as with a leveling off of cross-section at energies above a few BEV.

TABLE IV. SUMMARY OF HIGH ENERGY NUCLEON-NUCLEUS CROSS-SECTION DATA

Reference	Source	Target	Incident Particle	Energy (BEV)	Cross-section (Barns)	Remarks
29	Chen, Leavitt and Shapiro	Be	p	.860	.169 ± .015	Absorption of protons from Cosmotron Beam
		C	p	.860	.209 ∓ .022	
		Al	p	.860	.394 ∓ .010	
		Cu	p	.860	.728 ∓ .017	
		Sn	p	.860	1.110 ∓ .030	
		Pb	p	.860	1.680 ∓ .040	
		*Fe	p	.860	.650 ∓ .020	
30	Coor, Hill Hornyak, Smith and Snow	Be	n	1.4	.190 ± .010	Absorption of neutrons produced from Cosmotron
		C	n	1.4	.200 ∓ .010	
		Al	n	1.4	.410 ∓ .021	
		Cu	n	1.4	.670 ∓ .034	
		Sn	n	1.4	1.160 ∓ .058	
		Pb	n	1.4	1.730 ∓ .087	
		Bi	n	1.4	1.790 ∓ .089	
		U	n	1.4	1.890 ∓ .090	
		*Fe	n	1.4	.650 ∓ .033	
27	Bowen, Di Corato, Moore and Tagliaferri	C	π^-	1.5	.240 ± .014	Cloud Chamber examination of Cosmotron Beam
		C	p	2.8	.230 ∓ .012	
		Fe	π^-	1.5	.705 ∓ .037	
		Fe	p	2.8	.690 ∓ .028	
		Pb	π^-	1.5	1.600 ∓ .095	
		Pb	p	2.8	1.630 ∓ .075	
31	Sinha and Das	Al	Cosmic	4	.383 ± .032	Cloud Chamber
		Cu	Ray	4	.793 ∓ .040	
		Pb	Flux	4	1.72 ∓ .14	
		*Fe		4	.680 ∓ .040	

TABLE IV. (cont'd)

Reference	Source	Target	Incident Particle	Energy (BEV)	Cross-section (Barns)	Remarks
32	Alexander and Yekutreli	C	n	5.0	.235 ± .016	
19		Al	n	5.0	.381 ∓ .027	
		Cu	n	5.0	.586 ∓ .025	
		Pb	n	5.0	1.670 ∓ .079	
		*Fe	n	5.0	.650 ∓ .040	
33	Ashmore, Coccini, Diddens and Wetherell	Be	p	24.2	.16 ± .01	Absorption of protons from CERN Accelerator
		C	p	24.2	.21 ∓ .01	
		Al	p	24.2	.37 ∓ .02	
		Cu	p	24.2	.71 ∓ .04	
		Cd	p	24.2	1.15 ∓ .06	
		Pb	p	24.2	1.70 ∓ .08	
		*Fe	p	24.2	.62 ∓ .04	
18	Brenner and Williams	Fe	p+π	50	.61 ± .03	Absorption of Cosmic Rays using counters
		Fe	n	50	.61 ∓ .04	
53	Cowan	Fe	p+π+n	>50	.58 ± .10	
	Present Work	Fe	p+π+n	>50	.56 ± .07	

* extrapolated

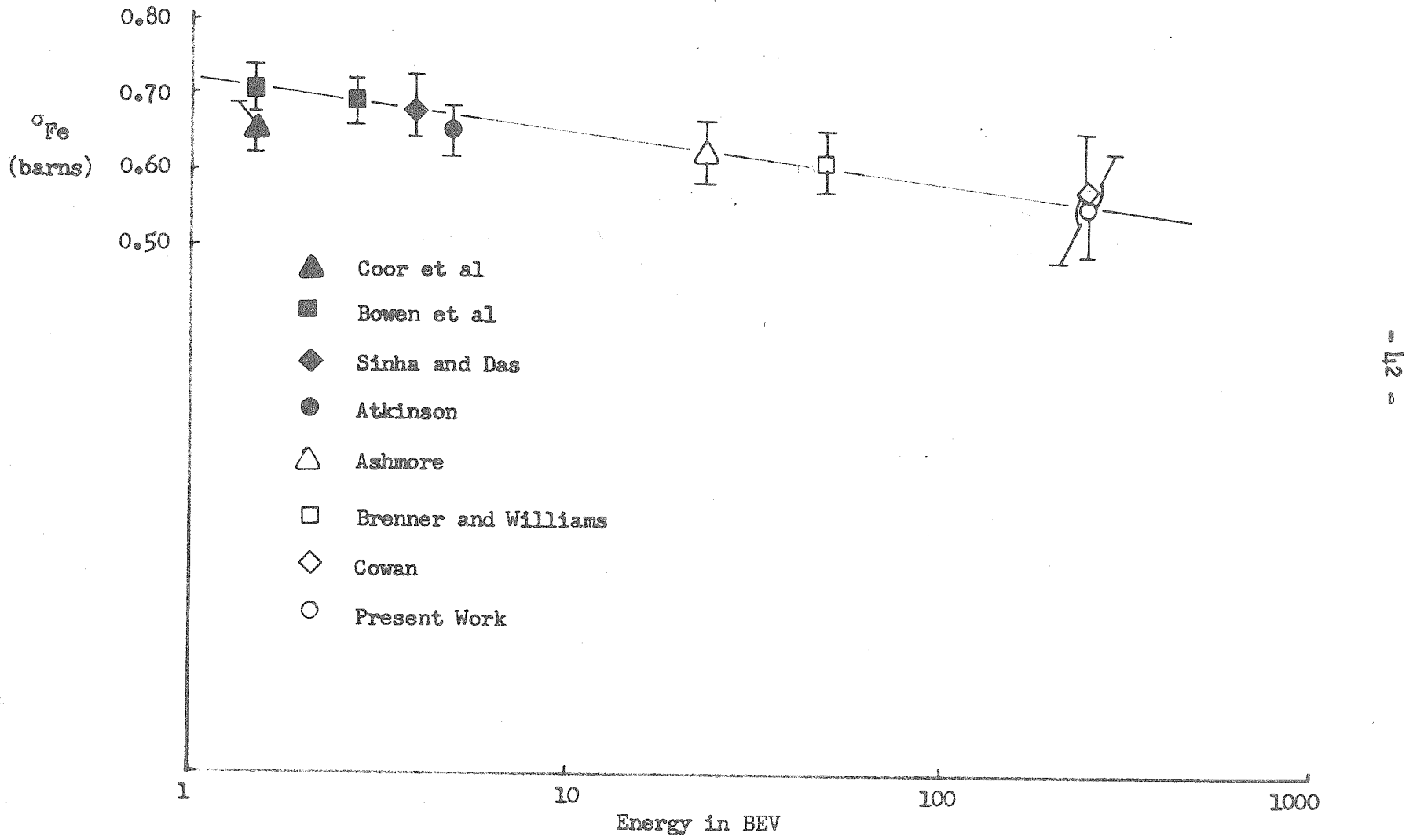

Fig. 9. Cross-section for inelastic scattering of nucleons by iron nuclei.

TABLE V. SUMMARY OF HIGH ENERGY NUCLEON-NUCLEON CROSS-SECTION DATA

(For Inelastic Scattering)

Reference	Source	Energy (BEV)	Cross-Section (mb)	Remarks
35 34	Dzhelepov, Moskalev and Medved (Dubna)	.410 .460 .500 .540 .580 .600 .620 .640 .660	3.9 ± 2.1 4.5 ± 2.0 6.9 ± 2.0 9.1 ± 2.1 12.6 ± 2.1 13.6 ± 2.1 15.6 ± 2.1 16.8 ± 2.1 18.4 ± 2.1	σ_{pp} obtained by subtracting $\sigma_{elastic}$ from σ_{total}.
36 34	Bogachev and Vzorov (Dubna)	.460 .560 .660	3.6 ± 0.7 8.8 ± 0.9 16.7 ± 1.2	σ_{pp} obtained by subtracting $\sigma_{elastic}$ (Ref. 36) from σ_{total} (Ref. 35).
37 34	Smith, McReynolds and Snow (Cosmotron)	.440 .590 .800 1.000	3.5 ± 2.3 10.8 ± 3.6 25.5 ± 2.8 28.8 ± 3.2	σ_{pp} obtained by subtracting $\sigma_{elastic}$ (Ref. 37) from σ_{total} (Ref. 38).
39 34	Batson, Culwick, Riddeford and Walker (Brookhaven Cloud Chamber)	.650	14.4 ± 1.4	
40	Morris, Fowler and Garrison (Brookhaven Cloud Chamber)	.800	24.3 ± 3	
41 34	Hughs, March, Muirhead and Lark (Bevatron Emulsion)	.925	33 ± 3	

Reference	Source	Energy (BEV)	Cross-section (mb)	Remarks
42 34	Fowler, Shutt, Thorndike and Whittemore (Cosmotron Cloud Chamber	1.5	27 ± 3	
43 34	Block et al. (Cosmotron Cloud Chamber)	2.75	26 ± 3	
31	Sinha and Das	4	27 ± 6	Reduced from $\overline{\sigma}_{Fe}$
32	Atkinson	5	24 ± 5	Reduced from $\overline{\sigma}_{Fe}$
44	Wright, Saphir, Powel, Maenchen and Fowler (Bevatron Cloud Chamber)	5.3	27 ± 6	σ_{pp} obtained by subtracting $\sigma_{elastic}$ from σ_{total}.
45	N. P. Bogachev et al.	9.4	28 ± 8	Obtained by normalizing total cross-section from Ref. 45 to Ref. 46.
47	Bogachev, Bunyatov, Merekov and Siderov	9	30 ± 4	σ_{pp} obtained by subtracting $\sigma_{elastic}$ from σ_{total}.

TABLE V (cont'd)

Reference	Source	Energy (BEV)	Cross-section (mb)	Remarks
33	Ashmore, Coccini, Diddens and Wetherell	24.4	22 + 4	Reduced from $\bar{\sigma}_{Fe}$
18	Brenner and Williams	50	21 $\pm$ 4	Reduced from $\bar{\sigma}_{Fe}$
53	Cowan	> 50	19 $\pm$ 7	Reduced from $\bar{\sigma}_{Fe}$
	Present Work	> 50	18 $\pm$ 5	Reduced from $\bar{\sigma}_{Fe}$

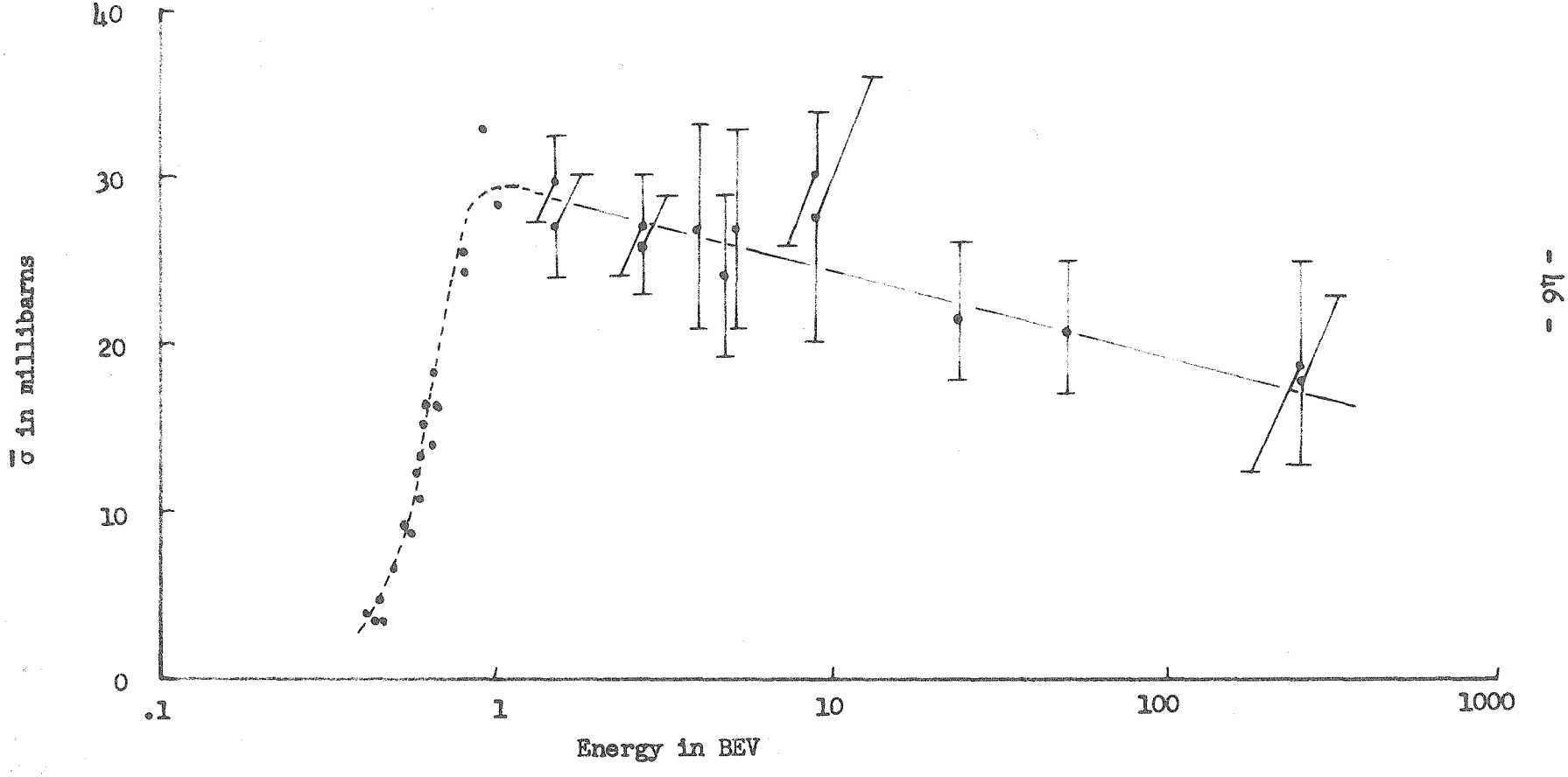

Fig. 10. Nucleon-nucleon cross-section for inelastic scattering

C. Discussion of the "Knock On" Events

As described in section III-A, certain events were studied in which a single secondary, emitted within a few degrees of the line of flight of the primary, contained a major share of the energy of the primary. A total of 31 events were tabulated, 12 with neutral and 19 with charged secondaries in the following sequence:

Primary	Secondary	Number
charged	charged	18
charged	neutral	8
neutral	charged	1
neutral	neutral	3

The range of the secondaries were measured and log N plotted as a function of range in Fig. 11. As can be seen from the figure, the ranges of the charged events are consistent with the expected distribution for charged nucleons and the neutrals with a mixture of γ-rays and neutrons. The γ-rays are probably the result of π^o decays since in the identification of the primary event, several particles are emitted. The falling off of the curves at longer values of x is to be expected considering the short gate length for many of the secondaries.

Because of the small number of events and the short gate length no quantitative information may be obtained concerning the ratios of protons or π^o's to charged π's. Qualitatively, however, one would expect approximately equal numbers of π^o, π^+ and π^- and also equal numbers of protons and neutrons. Roughly, even assuming a major portion of the charged secondaries are π mesons, extrapolating the number of neutrals back to the origin indicates an

excess of π^{o}'s to the π^{+} and π^{-}, although this is compensated somewhat by the smaller value of the ratio of gate-length to mean free path for the charged mesons compared to the γ-rays.

One point of interest however, is the small number of such events observed. In all approximately 600 interactions were observed with primaries over 50 BEV and of these, only 31 were observed as the type in which the secondary received a major portion of the energy, approximately 5% of the total.

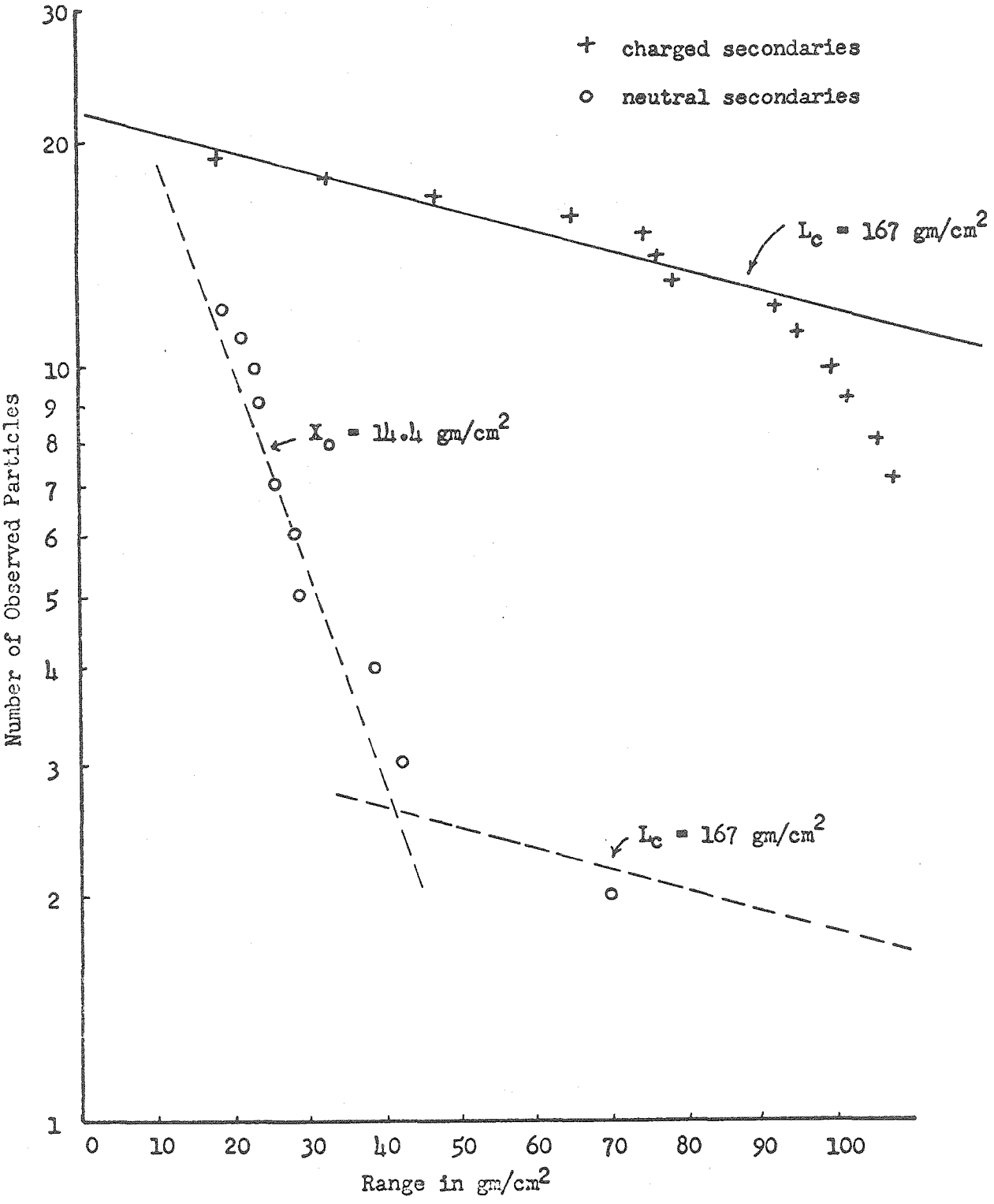

Fig. 11. Number of "knock-on" secondaries as a function of range.

VI. ABSOLUTE INTENSITY OF PENETRATING COMPONENT WITH ENERGIES IN EXCESS OF 50 BEV

A. Angular Distribution of Cosmic Ray Particles Greater than 50 BEV

In order to calculate the range of particles of energy greater than 50 BEV, it was necessary to measure the angle between the trajectory of the primary particles and the normal to the plates. In practice, the secant of the angle is measured rather than the angle itself as described in section III-C and Appendix B. The average value of $\sec\theta$ obtained for 551 events having a median energy of approximately 250 BEV and a minimum energy of 50 BEV was found to be 1.034. Table VI shows the distribution of events as a function of $\sec\theta$.

Since the efficiency of the cloud chamber will be a function of θ due to the angular dependence of the aperture for inclusion of an event under the criteria for selection of events (section III-A) it is necessary to correct the distribution obtained in order to determine the true angular dependence of the incident flux.

Let $J(\theta)$ be the intensity of the primary beam in the direction at an angle θ to the vertical, i.e., let $J(\theta)d\sigma d\omega$ represent the number of particles per unit time incident upon the element of area $d\sigma$ from a direction θ within the element of solid angle $d\omega$.

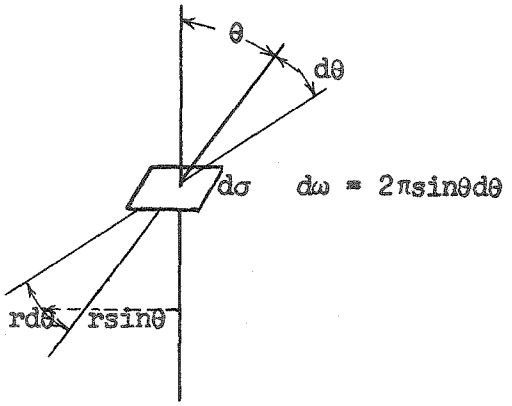

The number of particles per unit time striking an elemental area $d\sigma$ at an angle θ within an angle $d\theta$ will be

$$dN = J(\theta)\, 2\pi \sin\theta d\theta d\sigma \tag{26}$$

Let the coordinates of the elemental area be (x, y). For a given location of $d\sigma$ and a given value of θ, the fraction of incident particles which pass through the boundaries of the chamber bottom is $f(\theta, x, y)$, i.e., $f(\theta, x, y)$ is the efficiency of the chamber to detect particles striking the top plate at x, y, and at an angle θ. For a fixed value of θ and $d\theta$, the total flux observed will then be

$$\Phi(\theta, d\theta) = 2\pi \sin\theta J(\theta) d\theta \int\int f(\theta, x, y) dxdy \tag{27}$$

where the integral is taken over the top surface of the chamber. The quantity under the integral sign can be defined as the aperture of the chamber for a given angle of incidence:

$$A(\theta) \equiv \iint f(\theta, x, y)\, dxdy \tag{28}$$

Looking down along the normal to $d\sigma$, the particles passing through $d\sigma$ at an angle θ will form a circle in the plane of the bottom of the chamber or radius $r(\theta)$ centered at (x,y). From Fig. 12 it is apparent

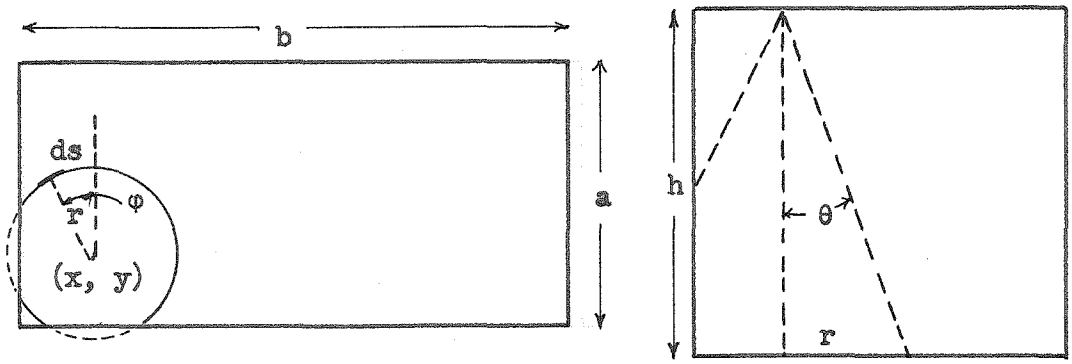

(a) Top Projection (b) Front Projection

Fig. 12. Projection of Path of Particles Incident in Direction θ.

that

$$r = h\tan\theta \tag{29}$$

Also it can be seen that f(r, x, y) (here, $r(\theta)$ is substituted for θ as the independent variable) will be equal to the fraction of the circle included in the allowed boundaries.

The efficiency, f(r, x, y) using the notation of Fig. 12a will be:

$$f(r, x, y) = \frac{\int ds}{2\pi r} = \frac{1}{2\pi} \int_0^{2\pi} g(\phi, r, x, y)\, d\phi \tag{30}$$

where $g(\phi, r, x, y)$ defines that part of the circle included within the boundary. The aperture A defined by Eq. 28 thus becomes

$$A = \frac{1}{2\pi} \iiint g(\phi, r, x, y)\, dx\, dy\, d\phi$$

Since ϕ, x and y are all independent variables, the order of integration can be interchanged. For a given value of ϕ, $g(\phi, r, x, y)$ can be thought of as the efficiency of the chamber in detecting particles incident at (x, y) for a particular ϕ and $r(\theta)$. For convenience a different aperture may be defined:

$$I(\phi, r) \equiv \iint g(\phi, r, x, y)\, dx\, dy \tag{31}$$

From symmetry, $I(\phi, r)$ need only be determined for values of ϕ between 0 and $\pi/2$, hence

$$A = \frac{2}{\pi} \int_0^{\pi/2} I(\phi, r)\, d\phi \tag{32}$$

By inspection, for $0 \leq \phi \leq \tan^{-1} b/a$

$$I(\phi, r) = \begin{cases} ab - rb\cos\phi - ra\sin\phi + \frac{1}{2}r^2\sin 2\phi & \text{if } \cos\phi \leq a/r \\ 0 & \text{if } \cos\phi \geq a/r \end{cases}$$

for $\tan^{-1} b/a \leq \phi \leq \pi/2$

$$I(\phi, r) = \begin{cases} ab - rb\cos\phi - ra\sin\phi + \frac{1}{2} r^2 \sin 2\phi & \text{if } \sin\phi \leq b/r \\ 0 & \text{if } \sin\phi \geq b/r \end{cases}$$

Integrating $I(\phi, r)$ as indicated in Eq. 32

for $r \leq a$

$$A = ab - \frac{r}{\pi}(2a + 2b - r)$$

for $a \leq r \leq b$

$$A = ab\left(1 - \frac{2}{\pi}\cos^{-1}\frac{a}{r}\right) - \frac{2}{\pi}\left[\frac{1}{2}a^2 + rb - b\,(r^2 - a^2)^{\frac{1}{2}}\right]$$

for $b \leq r \leq a^2 - b^2$

$$A = \frac{2}{\pi}\left[ab\left(\sin^{-1}\frac{b}{r} - \cos^{-1}\frac{a}{r}\right) + b(r^2 - a^2)^{\frac{1}{2}} + a(r^2 - b^2)^{\frac{1}{2}} - \frac{1}{2}(a^2 + b^2 + r^2)\right]$$

for $r \geq (a^2 + b^2)^{\frac{1}{2}}$ $A = 0$

The value of A/ab, i.e. the efficiency of the chamber is plotted as a function of θ in Fig. 13.

From Eq. 27 it is seen that the actual flux will be related to the observed flux by

$$J(\theta) = \frac{\Phi(\theta, d\theta)}{2\pi A d(\cos\theta)} \tag{33}$$

Table VI gives the data obtained for $\Phi(\theta, d\theta)$ and the resultant values of $J(\theta)$. These are tabulated in terms of $\sec\theta$. Since the value of $\sec\theta$ measured for each event was rounded to the nearest hundredth, $d(\sec\theta) = .01$ with the exception of the value for $\sec\theta = 1.00$ where $d(\sec\theta) = .005$. The increment of solid angle, θ $\sin\theta d\theta$ is thus

$$2\pi d(\cos\theta) = \frac{2\pi}{\sec^2\theta}\, d(\sec\theta) \tag{34}$$

If it is assumed that the flux distribution has the form*

$$J(\theta) = ke^{-n\sec\theta} \tag{35}$$

the best value of n can be calculated from the experimental data by making a least squares fit between the line

$$y_i = ax_i + b$$

where $y_i = \ln J(\theta)$ $\qquad a = -n$

$x_i = \sec\theta_i - 1$ $\qquad b = \ln k - n$

and the corrected values of $J(\theta_i)$ and x_i. The value of n obtained by this method is $n = 9.0 \pm 1.1$ where the error indicated is the standard deviation in n as estimated by the deviations of the experimental points from the straight line for $n = 9.0$; this error does not include the errors in the individual measurements of $J(\theta)$. The experimental points along with this estimate of $J(\theta)$ are plotted in Fig. 14.

---

*The assumption of this form for the flux distribution comes from the following reasoning:

Let $J(h, \theta)$ be the distribution function for the class of particles of interest at a depth h in the atmosphere. If the mean free path for these particles is L_c, the attenuation of the flux after passing through a thickness of air L would be e^{-L/L_c}. For particles incident at a direction θ, $L = h\sec\theta$ and

$$J(h, \theta) = J(0, \theta)e^{-h\sec\theta/L_c} \tag{36}$$

If it is assumed that the flux distribution at the top of the atmosphere is isotropic and that the secondary particles have very nearly the same direction of their primaries, the form of the distribution function would be that given by Eq. 35.

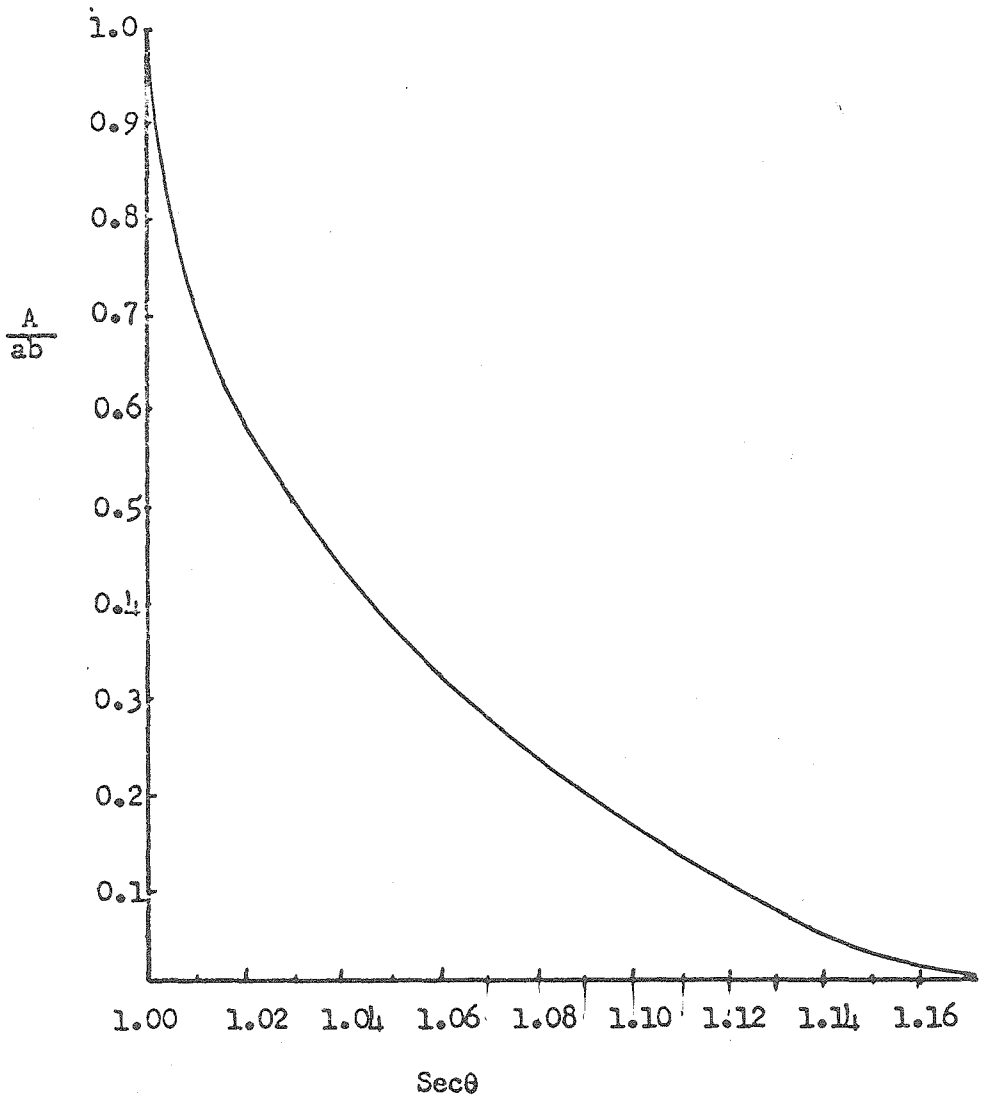

Fig. 13. Geometric Efficiency of 5' X 5' Cloud Chamber

TABLE VI. ANGULAR DISTRIBUTION OF PARTICLES WITH ENERGIES GREATER THAN 50 BEV

Sec θ	θ	d(cosθ)	r (cm)		A/ab	ab/A	$J(\theta)\frac{2\pi ab}{A}$
1.00	$(0\text{-}5)^{\circ}$	.005	0-15	103	.78	132	264
1.01	$8^{\circ}5'$	.0098	21	101	.70	144	147
1.02	$11^{\circ}22'$	.0096	30	105	.59	178	185
1.03	$13^{\circ}52'$	.0094	36	55	.51	108	115
1.04	$15^{\circ}56'$	.0092	42	42	.44	95	103
1.05	$17^{\circ}45'$	.0091	48	27	.37	73	80
1.06	$19^{\circ}22'$	.0089	53	28	.31	90	101
1.07	$20^{\circ}50'$	.0087	57	23	.27	85	98
1.08	$22^{\circ}12'$	.0086	61	20	.24	83	96
1.09	$23^{\circ}27'$	.0084	65	13	.20	65	78
1.10	$24^{\circ}37'$	.0083	68	9	.17	53	64
1.11	$25^{\circ}44'$	.0081	72	7	.14	50	62
1.12	$26^{\circ}46'$	.0080	75	6	.11	55	68
1.13	$27^{\circ}45'$	.0078	80	4	.08	50	64
1.14	$28^{\circ}42'$	.0076	83	2	.05	40	53
1.15	$29^{\circ}35'$	.0075	86	2	.03	30*	---
1.16	$30^{\circ}27'$	.0074	89	1	.02	20*	---
1.17	$31^{\circ}17'$	.0073	91	3	.01	10*	---

*extrapolated

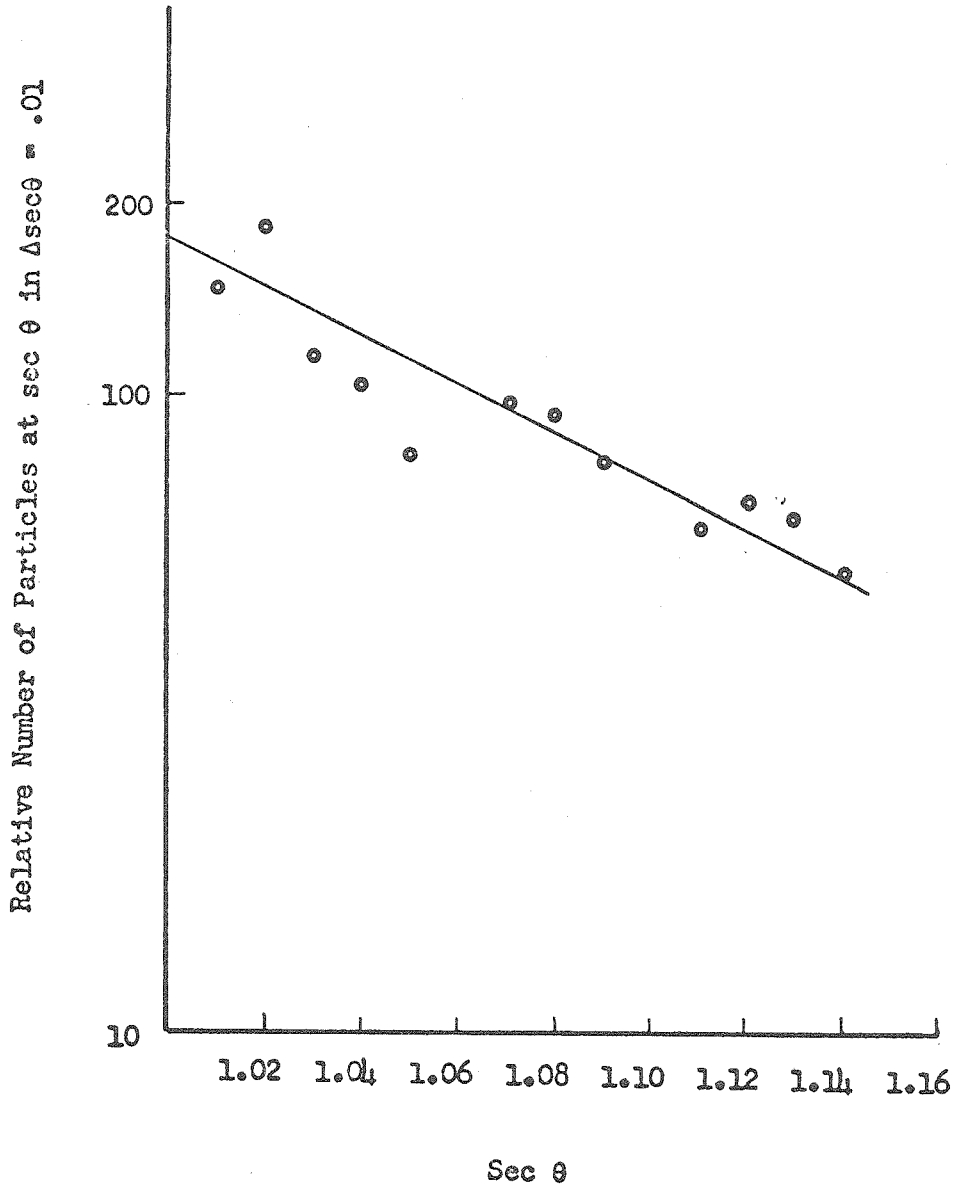

Fig. 14. Anguler distribution of particles with energies greater than 50 BEV.

B. Minimum Absolute Intensity of Cosmic Ray Particles Greater Then 50 BEV

Angular measurements were made for 551 events of the 606 events tabulated. Correcting for the efficiency of the chamber for each value of $\sec\theta$, the efficiency of tabulation (estimated as 80%) and the number of events for which angular measurements were made, the number of particles incident upon the chamber top surface during the experiment was 1850. The total running time to obtain this data was 6,700 hours and the area of the chamber top surface is .9 m^2. Thus the flux of particles greater than 50 BEV is found to be .31 particles $hr^{-1}m^2$. The constant in Eq. 35 may be determined by integrating $J(\theta)$ over the upper hemisphere:

$$\frac{dN}{d\sigma} = 2\pi \int J(\theta) \sin\theta d\theta \qquad (36)$$

$$= 2\pi k \int_0^1 e^{-n\sec\theta} d(\cos\theta)$$

Substituting $s = \sec\theta$, $d(\cos\theta) = -\frac{1}{s^2} ds$

or

$$\frac{dN}{d\sigma} = 2\pi k \int_1^\infty \frac{1}{s^2} e^{-ns} ds \qquad (37)$$

This integral, called the Gold Integral is shown by Rossi[1] for $n >> 1$ to be

$$\mathcal{E}_1(n) \equiv \int_1^\infty \frac{e^{-ns}}{s^2} ds \approx \frac{e^{-n}}{n} \qquad (38)$$

For $n = 9.0$, $\mathcal{E}_1(n) = 1.1 \times 10^{-5}$ and

$$k = \frac{.31}{2\pi \, \mathcal{E}_1(9.0)} = 4.5 \times 10^3 \ m^2 \ hr^{-1} \ steradian^{-1}$$

$$= 1.3 \ m^{-2} \ sec^{-1} \ steradian^{-1}$$

The experimentally determined expression for the flux density is

$$J(\theta) = 1.3\ e^{-9.0\ \sec\theta}\ m^{-2}\ sec^{-1}\ steradian^{-1} \qquad (39)$$

Each event observed in the chamber resulted from a particle of energy greater than 50 BEV. These particles could have been part of the primary cosmic-rays or a secondary from an interaction in the atmosphere. In either case, every interaction observed must have resulted from a primary cosmic-ray with energy greater than 50 BEV. From the previous analysis, if the primary cosmic-ray beam is isotropic above the atmosphere, the quantity n in Eq. 35 is the number of mean free paths of air above the chamber for vertically incident particles. This mean free path is not the interaction length for multiple particle production but the thickness of air required to reduce the number of particles having 50 BEV of energy or greater by 1/e. If the number of mean free paths is taken as 9.0, then comparison of Eqs. 36 and 39 gives the minimum value for the flux of particles with energies greater than 50 BEV incident upon the atmosphere as $N_E(50) = 1.3\ m^{-2}\ sec^{-1}\ steradian^{-1}$.

The most significant error in $N_E(50)$ results in the determination of n. The absorption thickness (mean free path for complete removal of incident particles) averaged over the entire cosmic ray spectrum above a few BEV has been shown to be ~120 gm/cm^2 (1). From Eq. 36 $n = h/L_c = 1030/120 = 8.7$. The results of this experiment predict as the nucleon-nucleon cross-section 18 mb which, using the transparency curves of Alexander and Yekutreli(19) would predict a similar value as the mean free path for multiple particle production

and hence an absorption thickness greater than this value. As described in the following section, at higher energies the absorption thickness and the collision thickness may be very nearly equal, making the value of $n = 9.0$ reasonable.

From Peters[28] the observed flux of primary protons of energy greater than 50 BEV is 75 particles m^{-2} sec^{-1} $steradian^{-1}$ and for energies greater than 100 BEV, 20 particles m^{-2} sec^{-1} $steradian^{-1}$.

C. Significance of the Ratio of Neutrons to Protons--Elasticity

It has been generally assumed that deep in the atmosphere for sufficiently high energies, the integrated flux due to neutrons and protons would be approximately equal. This is a consequence of the observation that all of the neutrons and practically all of the protons detected at moderate altitudes are secondary particles generated in nuclear interactions at some altitude above the place of observation. Therefore, the energy spectrum of these neutrons (or protons) is related to the energy spectrum of the neutrons (or protons) produced in nuclear interactions which should be the same for protons and neutrons at energies where the ionization loss of the protons is negligible. The relative numbers of particles should depend only upon the probability of producing a given nucleon. For a single nucleon-nucleon interaction one particle of energy E_p disappears from the beam and two particles reappear with an average energy E_s. One of the secondaries will have the charge of the incident nucleon, the other will have the charge of the target nucleon.

Since the nuclei which constitute the atmosphere have equal numbers of neutrons and protons, either of these are equally likely as the target nucleon. On the average an incident proton $\rightarrow$ 3/2 p + 1/2 n and an incident neutron $\rightarrow$ 1/2 p + 3/2 n. By tracing the secondaries produced from a primary proton it can be seen that within a very few interactions the ratio of protons to neutrons would be very nearly one if this were the only process involved. The number of nucleons in any given energy range does not necessarily increase by this process since with each interaction the average energy of the secondaries can be considerably less than the energy of the primary.

If one considers only particles above some threshold E_o, in this case 50 BEV, the preceding argument could be invalid for highly inelastic interactions, i.e. when the average of E_s is reduced to less than E_o within 1 or 2 interaction lengths. In this case, the importance of the secondaries would be smaller compared to primaries resulting in a larger proportion of protons to neutrons. Hence, the ratio of neutrons to protons should be dependent upon some parameter which is a measure of the energy lost to the nucleons in a collision.

Most of the data available on elasticity results from detailed examination of the energy balance in stars produced in nuclear emulsions[49-52]. In these experiments, the quantities measured are the energy of the incident particles and the energies of the secondaries produced. Hence, it has been more convenient to define a parameter which is a measure of the inelasticity, i.e. the fraction of the energy available for secondary particle production. Since the various definitions of inelasticity used differ in slight details,

the following definition of elasticity and inelasticity are proposed:

$$\mathcal{E} = \text{Elasticity} = \frac{\text{Kinetic Energy of Incident Nucleons after Collision}}{\text{Kinetic Energy of Primary Nucleons Before Collision}} \tag{40}$$

$$k = \text{Inelasticity} = \frac{\text{Total Energy of Particles Produced}}{\text{Kinetic Energy of Primary Nucleons Before Collision}} \tag{41}$$

From conservation of energy:

$$\mathcal{E} + k = 1 \tag{42}$$

These definitions are unambiguous so long as nucleon-anti-nucleon pair production is not a significant process and the energies are referred to the center of mass system. At energies large enough for such pair production, the identification of the incident nucleons after collision is impossible; however, if the mechanism of nucleon-anti-nucleon pair production were known, the distribution of energy between the nucleons would give an estimate of $\mathcal{E}$ and k.

If these quantities are not referred to the center-of-mass system an ambiguity results from the difference between the kinetic energy of the incident nucleon in the laboratory system and the fraction of the kinetic energy available for secondary particle production. In the center-of-mass system if the two colliding particles come to rest, all of the incident kinetic energy will be converted to secondary particles in which case $k_c = 1$ and $\mathcal{E}_c = 0$. However in the laboratory system $\mathcal{E}_L = \frac{1}{\gamma_c - 1}$ and $k_L = \frac{\gamma_c}{\gamma_c - 1}$ where $\gamma_c = 1/\sqrt{1-\beta_c^2}$, and β_c^2 is the velocity of the center of mass (see Appendix A). At

sufficiently high energies this difference is entirely negligible. However, if the elasticities are small, the ratio of $\mathcal{E}_c$ to $\mathcal{E}_L$ could be considerable. This value of $\mathcal{E}$ corresponds to the smallest elasticity possible in the laboratory system. For a cutoff energy of 50 BEV, $\mathcal{E}_{min} = .02$ and $E_p = 5 \times 10^3$ BEV. If indeed $\mathcal{E}$ were this small, the secondary particles would comprise a very small portion of the observed nucleon flux. If the threshold energy for inclusion of an event is small, say 1 BEV, $\mathcal{E}_{min} = .3$ and the contribution to the flux from the secondaries would be significant. At lower energies, the large difference between the interaction thickness and the absorption thickness indicates larger elasticities. At higher energies, as previously discussed, the result that the interaction cross-section and the absorption cross-section are nearly the same lends emphasis to the assumption that the elasticity is small.

With these considerations in mind, it is possible to derive an approximate expression for the ratio of neutrons to protons as a function of depth in the atmosphere under appropriate assumptions. For convenience, only the vertical component of the incident flux will be considered.

Let: $j^{(p)}(E, x)$ = the number of protons present at a depth x in the atmosphere with an energy greater than E.

$j^{(n)}(E, x)$ = the number of neutrons present at a depth x in the atmosphere with an energy greater than E.

$J(E)$ = the number of protons at the top of the atmosphere with an energy greater than E.

$P'(E, E^*)$ = the probability that one secondary nucleon from a single nucleon-nucleon collision will possess an energy greater than E for an incident nucleon energy E^*.

$P''(E, E^*)$ = the probability that both secondary nucleons from a single nucleon-nucleon collision will possess an energy greater than E for an incident nucleon energy E^*.

All energies are measured in the laboratory system and x and L_c are in units of gm/cm^2. The probability of a particle interacting in a distance dx is just dx/L_c. L_c will be taken as being independent of energy. Although this is probably not a valid assumption, at worst, L_c varies logarithmically with energy whereas the intensity will vary exponentially, hence over the region for which there is significant flux, L_c is reasonably constant. The variation with depth in the atmosphere of $j^{(p)}(E, x)$ and $j^{(n)}(E, x)$, neglecting ionization loss for the protons, will be:

$$\frac{\partial j^{(p)}(E, x)}{\partial x} = -\frac{j^{(p)}(E, x)}{L_c} + \frac{3}{4}\int_E^\infty \frac{\partial j^{(p)}(E^*, x)}{\partial E^*} \frac{[P'(E, E^*)+P''(E, E^*)]}{L_c} dE^*$$

$$+ \frac{1}{4}\int_E^\infty \frac{\partial j^{(n)}(E^*, x)}{\partial E^*} \frac{[P'(E, E^*)+P''(E, E^*)]}{L_c} dE^* \qquad (43a)$$

$$\frac{\partial j^{(n)}(E, x)}{\partial x} = -\frac{j^{(n)}(E, x)}{L_c} + \frac{3}{4}\int_E^\infty \frac{\partial j^{(n)}(E^*, x)}{\partial E^*} \frac{P'E, E^*)+P''(E, E^*)}{L_c} dE^*$$

$$+ \frac{1}{4}\int_E^\infty \frac{\partial j^{(p)}(E^*, x)}{\partial E^*} \frac{P'(E, E^*) + P''(E, E^*)}{L_c} dE^* \qquad (43b)$$

Defining energies E_p', E_p'', E_n' and E_n'' such that

$$j^{(p)}(E_p', x) = \int_{E_o}^{\infty} \frac{\partial j^{(p)}(E^*, x)}{\partial E^*} P'(E_o, E^*)\, dE^* \tag{44a}$$

$$j^{(p)}(E_p'', x) = \int_{E_o}^{\infty} \frac{\partial j^{(p)}(E^*, x)}{\partial E^*} P''(E_o, E^*)\, dE^* \tag{44b}$$

$$j^{(n)}(E_n', x) = \int_{E_o}^{\infty} \frac{\partial j^{(n)}(E^*, x)}{\partial E^*} P'(E_o, E^*)\, dE^* \tag{44c}$$

$$j^{(n)}(E_n'', x) = \int_{E_o}^{\infty} \frac{\partial j^{(n)}(E^*, x)}{\partial E^*} P''(E_o, E^*)\, dE^* \tag{44d}$$

where E_o is the threshold for inclusion of an event, Eqs. 43 become

$$\frac{\partial j^{(p)}(E_o, x)}{\partial x} = -\frac{j^{(p)}(E_o, x)}{L_c} + \frac{3}{4}\frac{j^{(p)}(E_p', x)}{L_c} + \frac{3}{4}\frac{j^{(p)}(E_p'', x)}{L_c} + \frac{1}{4}\frac{j^{(n)}(E_n', x)}{L_c} + \frac{1}{4}\frac{j^{(n)}(E_n'', x)}{L_c} \tag{45a}$$

$$\frac{\partial j^{(n)}(E_o, x)}{\partial x} = -\frac{j^{(n)}(E_o, x)}{L_c} + \frac{3}{4}\frac{j^{(n)}(E_n', x)}{L_c} + \frac{3}{4}\frac{j^{(n)}(E_n'', x)}{L_c} + \frac{1}{4}\frac{j^{(p)}(E_p', x)}{L_c} + \frac{1}{4}\frac{j^{(p)}(E_p'', x)}{L_c} \tag{45b}$$

We shall try to find solutions to Eqs. 45 of the following form:

$$j^{(p)}(E, x) = F^{(p)}(E)\, u^{(p)}(x) \tag{46a}$$

$$j^{(n)}(E, x) = F^{(n)}(E)\, u^{(n)}(x) \tag{46b}$$

Substituting Eqs. 46 into Eqs. 45

$$\frac{du^{(p)}(x)}{dx} = -\frac{u^{(p)}(x)}{L_c}\left[1 - \frac{3}{4}\frac{F^{(p)}(E_p') + F^{(p)}(E_p'')}{F^{(p)}(E_o)}\right] + \frac{u^{(n)}(x)}{L_c}\left[\frac{1}{4}\frac{F^{(n)}(E_n') + F^{(n)}(E_p'')}{F^{(p)}(E_o)}\right] \tag{47a}$$

$$\frac{du^{(n)}(x)}{dx} = -\frac{u^{(n)}(x)}{L_c}\left[1 - \frac{3}{4}\frac{F^{(n)}(E_n') + F^{(n)}(E_n'')}{F^{(n)}(E_o)}\right] + \frac{u^{(p)}(x)}{L_c}\left[\frac{1}{4}\frac{F^{(p)}(E_p') + F^{(p)}(E_p'')}{F^{(n)}(E_o)}\right] \tag{47b}$$

For convenience, the quantities α_n, α_p, β_n and β_p will be defined such that Eqs. 47 become

$$\frac{du^{(p)}(x)}{dx} = -\alpha_p u^{(p)}(x) + \beta_n u^{(n)}(x) \tag{48a}$$

and

$$\frac{du^{(n)}(x)}{dx} = -\alpha_n u^{(n)}(x) + \beta_p u^{(p)}(x). \tag{48b}$$

The definitions of the α's and β's are obtained by comparison of Eqs. 47 and 48. Eqs. 48 may be solved by the change of variables:

$$u^{(p)}(x) = k^{(p)}(x)\, e^{-\alpha_p x} \tag{49a}$$

$$u^{(n)}(x) = k^{(n)}(x)\, e^{-\alpha_n x} \tag{49b}$$

Eqs. 48 become:

$$\frac{dk^{(p)}(x)}{dx} = \beta_n e^{-(\alpha_n - \alpha_p)x} k^{(n)}(x) \tag{50a}$$

$$\frac{dk^{(n)}(x)}{dx} = \beta_p e^{-(\alpha_p - \alpha_n)x} k^{(p)}(x) \tag{50b}$$

Using the boundary conditions at the top of the atmosphere, namely $u^{(p)}(0) = 1$ and $u^{(n)}(0) = 0$, these two simultaneous differential equations may easily be solved, yielding for $u^{(p)}(x)$ and $u^{(n)}(x)$

$$u^{(p)}(x) = e^{-\alpha_p x} \cosh\left(\frac{1}{2}\sqrt{(\alpha_p-\alpha_n)^2 + 4\beta_p\beta_n}\right) x \tag{51a}$$

$$u^{(n)}(x) = C_e^{-\alpha_n x} \sinh\left(\frac{1}{2}\sqrt{(\alpha_p-\alpha_n)^2 + 4\beta_p\beta_n}\right) x \tag{51b}$$

For $x \to \infty$, $u^{(p)}(x) \to u^{(n)}(x)$ or $C = 1$ and $\alpha_p = \alpha_n$. This is equivalent to saying that both neutrons and protons have the same form of the integral energy spectrum, i.e. $F^{(n)}(E) = F^{(p)}(E)$. Applying the boundary condition that at $x = 0$, $j^{(p)}(E, 0) = J(E)$, $F(E) = J(E)$. The resulting solutions to Eq. 43 are:

$$j^{(p)}(E_o, x) = J(E_o) \cosh(\beta x)\, e^{-\alpha x} \tag{52a}$$

$$j^{(n)}(E_o, x) = J(E_o) \sinh(\beta x)\, e^{-\alpha x} \tag{52b}$$

where

$$\beta = \frac{1}{4}\,\frac{J(E') + J(E'')}{J(E_o) L_c} \tag{53}$$

$$\alpha = \frac{1}{L_c} - 3\beta \tag{54}$$

It now remains to determine the quantities E' and E'' defined by Eq. 44.

$$J(E') = \int_{E_o}^{\infty} \frac{\partial J(E^*)}{\partial E^*}\, P'(E_o, E^*)\, dE^* \tag{55}$$

$$J(E'') = \int_{E_o}^{\infty} \frac{\partial J(E^*)}{\partial E^*}\, P''(E_o, E^*)\, dE^* \tag{56}$$

The quantities $P'(E_o, E^*)$ and $P''(E_o, E^*)$ will be related to the elasticity of the interaction and the distribution of the available kinetic energy between the two nucleons. The energy of a secondary nucleon in the laboratory system is related to its energy in the center-of-mass system by (see Appendix A)

$$\gamma_s = \gamma_c \gamma_s' + [(\gamma_c^2 - 1)(\gamma_s'^2 - 1)]^{\frac{1}{2}} \cos \theta_s' \tag{57}$$

where γ_s and γ_s' are the total energies of the secondary nucleon in the laboratory and the center-of-mass systems respectively, measured in units of Mc^2, $\gamma_c = 1/\sqrt{1 - \beta_c^2}$, β_c = velocity of the center-of-mass in units of c and θ_s' the angle of emission of the secondary in the center-of-mass system with respect to the line of flight of the incident nucleon.

The energy of the two secondaries is related to the energy of the incident particle by the definition of elasticity (Eq. 40).

$$\gamma_{s_1} + \gamma_{s_2} = \mathcal{E}(\gamma_p - 1) + 2 \tag{58}$$

The energy of the two secondaries will be similarly related to the energy of the incident nucleons in the center-of-mass system.

$$\gamma_{s_1}' + \gamma_{s_2}' = 2\,\mathcal{E}'(\gamma_p' - 1) + 2 \tag{59}$$

For any given model of the distribution in energy and space of the secondary nucleons in the center-of-mass system, the partition of the available energy between the two secondaries in the laboratory system can be determined. Several reasonable models are considered.

Case A. Let the two nucleons be distributed isotropically with a common energy and zero total linear momentum. Call s_1 the particle emitted in the forward hemisphere and s_2 the particle emitted in the backward hemisphere. The probability of s_1 being emitted in $d\Omega$ is $\frac{1}{2\pi} d\Omega = d(\cos\theta_{s_1}')$, i.e. all values of γ_{s_1} for $\cos\theta$ between 0 and 1 and all values of γ_{s_2} for $\cos\theta$ between 0 and -1 are equally probable. The relative probability for a particular value of γ_s as a function of γ_s is shown below. The ratio of the average energy of the higher energy secondary to the lower energy secondary is

$$\eta_a = \frac{\bar{\gamma}_{s_1}}{\bar{\gamma}_{s_2}} = \frac{\gamma_c\gamma_s' + \frac{1}{2}[(\gamma_c^2-1)(\gamma_s'^2-1)]^{\frac{1}{2}}}{\gamma_c\gamma_s' - \frac{1}{2}[\gamma_c^2-1)(\gamma_s'^2-1)]^{\frac{1}{2}}} \tag{60}$$

The maximum possible value of η_a is 3, the minimum value, 1.

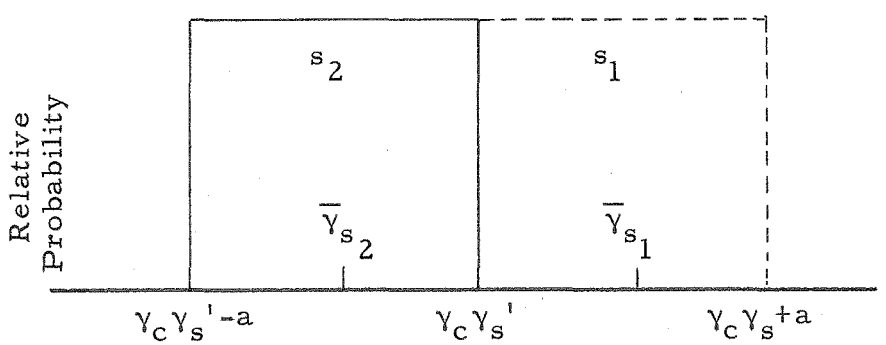

Case B. Let the two nucleons be distributed as $\cos^2\theta$ with a common energy and zero total linear momentum. Using the same notation as in Case A, the probability of s_1 being emitted in $d\Omega$ is $\frac{3}{2\pi}\cos^2\theta\, d\Omega = 3\cos^2\theta d(\cos\theta)$. The ratio of the higher energy secondary to the lower energy secondary is

$$\eta_b = \frac{\bar{\gamma}_{s_1}}{\bar{\gamma}_{s_2}} = \frac{\gamma_c\gamma_s' + \frac{3}{4}[\gamma_c^2-1)(\gamma_s'^2-1)]^{\frac{1}{2}}}{\bar{\gamma}_c\gamma_s' - \frac{3}{4}[\gamma_c^2-1)(\gamma_s'^2-1)]^{\frac{1}{2}}} \tag{61}$$

The maximum possible value of η_b is 7, the minimum value is 1.

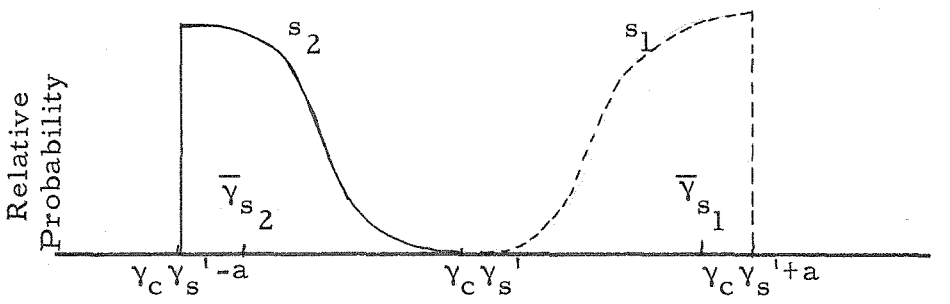

Case C. Let the two nucleons be distributed in any fashion with independent moments. In this case both particles can be either in the forward or backward hemisphere and hence $\bar{\gamma}_{s_1} = \bar{\gamma}_{s_2}$ or $\eta_c = 1$.

From the definitions of $\mathcal{E}$ and η, neglecting the rest masses of the nucleons compared to their kinetic energies, $\bar{\gamma}_{s_1} + \bar{\gamma}_{s_2} = \mathcal{E}\gamma_p$ and $\bar{\gamma}_{s_1}/\bar{\gamma}_{s_2} = \eta$, hence

$$\bar{\gamma}_{s_1} = \mathcal{E}\gamma_p \frac{\eta}{\eta+1} \quad \text{and} \quad \bar{\gamma}_{s_2} = \gamma_p \frac{\mathcal{E}}{\eta+1} \tag{62}$$

or

$$\gamma_p = \frac{\eta+1}{\eta} \frac{\bar{\gamma}_{s_1}}{\mathcal{E}} \quad \text{and} \quad \gamma_p = \frac{\eta+1}{\mathcal{E}} \bar{\gamma}_{s_2} \tag{63}$$

From the definitions of E' and E'' in Eqs. 44

$$E' = \frac{\eta+1}{\eta} \frac{E_o}{\mathcal{E}} \qquad E'' = \frac{\eta+1}{\mathcal{E}} E_o \tag{64}$$

Using as the integral energy spectrum of the primary protons $J(E) = E^{-1.5}$, the value of β in Eqs. 53 becomes

$$\beta = \frac{1}{4L_c} \left(\frac{\eta\mathcal{E}}{\eta+1}\right)^{1.5} \left[1 + \left(\frac{1}{\eta}\right)^{1.5}\right] \tag{65}$$

For a given value of β, the ratio of the values of $\mathcal{E}$ obtained using $\eta = 1$ ($\mathcal{E}_1$) to that obtained for $\eta = \infty$ ($\mathcal{E}_\infty$) is just $\mathcal{E}_1/\mathcal{E}_\infty = 1/2^{1/3} = .8$. Hence the worst possible choice for the value of η would result in a

maximum error in $\mathcal{E}$ of 20%. From examination of the cases discussed, η_{max} is probably near 3 or 4 and the maximum error in choosing η as 1 or ∞ is more nearly 10%. For the purpose of this paper, η will be taken as 1. This will result in an underestimate of $\mathcal{E}$ by no more than 10%.

The ratio of neutrons to protons at a depth x for energies greater than E_o will be, from Eqs. 52 and 65:

$$\mathcal{R}(E_o, x) \equiv \frac{j^{(n)}(E_o, x)}{j^{(p)}(E_o, x)} = \tanh(\beta x) \tag{66}$$

where $$\beta x = .18 \frac{x}{L_c} \mathcal{E}^{1.5} \tag{67}$$

The total intensity of protons and neutrons with energies greater than E_o is:

$$j^{(t)}(E_o, x) = J(E_o)e^{-(\alpha-\beta)x} \tag{68}$$

The coefficient $1/(\alpha-\beta)$ is the absorption coefficient and is related to the mean free path for interactions by the elasticity:

$$L_a = \frac{1}{\alpha-\beta} = L_c \left[\frac{1}{1 - .7\mathcal{E}^{1.5}}\right] \tag{69}$$

For small values of $\mathcal{E}$, $L_a \approx L_c$.

The results of Eqs. 52, 66 and 69 have been plotted in Figs. 15, 16 and 17. As can be seen from the equations and the figures, the predicted relative abundance of neutrons and protons in the atmosphere above a cut-off energy where the ionization loss of the protons is negligible is far different from that which is observed for all protons and neutrons. In the high energy region, the density of protons exceeds that of neutrons whereas at moderate energies,

due to the absorption of protons by electromagnetic processes, the converse is true.

In the statement of Eqs. 43a and 43b, nucleons resulting from meson-nucleon and from nucleon pair production were not included. If either of these processes is significant it would tend to equalize $j^{(p)}$ and $j^{(n)}$.

The contribution from the meson-nucleon interactions can be estimated by the following reasoning. Assuming that the multiplicity for meson production is $\sim E^{1/2}$ (E in BEV), the average energy of the mesons emitted from a nucleon-nucleon interaction with primary energy E will be $\sim E^{1/2}$. If an energy E' is required to have a significant probability of emitting a nucleon with energy greater than E_o, then the average meson energy for nuclear production must be E' or the energy of the nucleon creating the mesons must have energy greater than $E = E'^2$. The relative contribution from meson-nucleon interactions will be approximately the ratio of nucleons present at energy E'^2 to those present at E_o times the average meson multiplicity. E' is taken as $\frac{1}{\mathcal{E}} E_o$ where $\mathcal{E}$ is the elasticity observed in nucleon-nucleon interactions, $\mathcal{E} \approx .2$.

$$\frac{J(E'^2)}{J(E_o)} (\text{multiplicity}) = E' \left(\frac{E_o}{E'^2}\right)^{1.5} = \frac{E_o}{\mathcal{E}} \left(\frac{\mathcal{E}^2 E_o}{E_o^2}\right)^{1.5}$$

$$= \frac{\mathcal{E}^2}{E_o^{1/2}} < 1\% \qquad (57)$$

Thus the contribution to the observed nucleons from production by pi-mesons which themselves must have been produced from nucleon-nucleon interactions is probably negligible. This does not say, however, that the density of the π-mesons themselves is negligible as is usually assumed at lower energies. Pi-mesons disappear rapidly by spontaneous decay as they travel in the atmosphere. At

high energies, the relativistic increase of the mean life is sufficient to make the mean free path before decay long compared to the absorption thickness.

The possible problem from nucleon-pair production is more serious since in this case it is the nucleon-anti-nucleon pairs which directly add to $j^{(p)}$ and $j^{(n)}$ and not secondaries which they in turn cause. It is possible that at extremely high energies, say of the order of 10^6 BEV, such a process is significant, but at present there is no evidence for a contribution from this source in the 50-500 BEV region[48]. Because of the rapidly decreasing flux of incident protons at high energies, it is the processes which occur within a decade or so above the cutoff energy which will strongly affect the calculated distributions.

In characterizing any model for nucleon-nucleon interactions one can either study in detail a single interaction or try to predict some property averaged over many interactions such as meson-multiplicity, angular distribution of secondaries, average transverse momentum, elasticity, etc. From Figs. 15 and 17 it can be seen that the ratio of neutron to proton flux is highly dependent upon $\mathcal{E}'$ for low values of $\mathcal{E}$ and the ratio of absorption thickness to interaction length is highly dependent upon $\mathcal{E}'$ for larger values of $\mathcal{E}$, hence measurement of absolute intensities at sea level can provide good limits upon the elasticity. Unfortunately, there is no way of separating the charged pi-meson flux from the proton flux, hence these must be lumped together.

A total of 606 events were measured according to the criteria outlined in section III-A. Of these, 108 were the result of neutral primaries and 498 the result of charged primaries. During

the 6,700 hours of operation required to accumulate the data, the chamber was triggered by coincidence of three counters in each of two arrays mounted below the chamber. There was no selection made on the basis of the charge of the primary and hence the photographs probably represent an unbiased record of the ratio of neutral to charged particles incident upon the chamber. In the reduction of the data a decision had to be made for each event, namely whether the projected line of flight of the primary crosses plate 1 and 11 in the visible region of the chamber. For charged events, the line of flight of the primary could be easily projected through the chamber and the selection made in an unbiased manner. On the other hand, the line of flight of the neutrals had to be determined by reconstruction of the secondaries. Since the primary purpose of the experiment was to measure the cross-section, the inclusion of events with foreshortened gate lengths would represent a systematic error in that measurement; events which were in doubt were excluded. Hence the number of neutrals is subject to a systematic error in the direction of giving a smaller number. From the angular distribution of events, this bias is estimated at approximately 10%.

The ratio of neutrons to charged particles is found to be .22, thus the ratio of neutrons to protons has a maximum value of .22. The corresponding value for the elasticity from Eqs. 66 and 67 using the value of x/L_c obtained from the data on angular distribution is $.27 \pm .06$.

An upper limit of $\mathcal{E}$ may be determined from the relation between the absorption mean free path and the interaction mean free path (Eq. 69). The absorption mean free path in air, from

the data on angular distribution is found to be 115 ± 15 gm/cm^2 and the interaction mean free path corresponding to a mean free path of 167 ± 22 gm/cm^2 in iron is calculated to be 110 ± 15 gm/cm^2 or $L_a/L_c = 1.05 \pm .21$. This sets an upper limit for $\mathcal{E}$ at .45. The limits on the elasticity in nucleon-nucleon interactions is thus estimated at:

$$.27 \pm .06 \leq \mathcal{E} \lesssim .45$$

Most of the data presently available estimating the elasticity in nucleon-nucleon interactions are the result of nuclear-emulsion work. In these experiments the ratio of the estimated energies of the secondaries in a star to the primary is calculated and a value for the inelasticity k is determined. The energy of the primary is usually determined from the angular distribution of the secondaries and the total energy of the secondaries measured by ionization, scattering and range of the individual tracks. This method gives the maximum value of the inelasticity. Because of the large uncertainties in this method and the probable statistical behavior of the inelasticity, this method can give meaningful results only when averaged over a large number of events. The most significant study thus far undertaken is an analysis of 57 interactions reported by Shein et al.[52] in which the value of the inelasticity is $\langle k \rangle \approx 0.50$ with a lower limit of 0.25. This corresponds to $\langle \mathcal{E} \rangle \approx 0.50$ with an upper limit of 0.75.

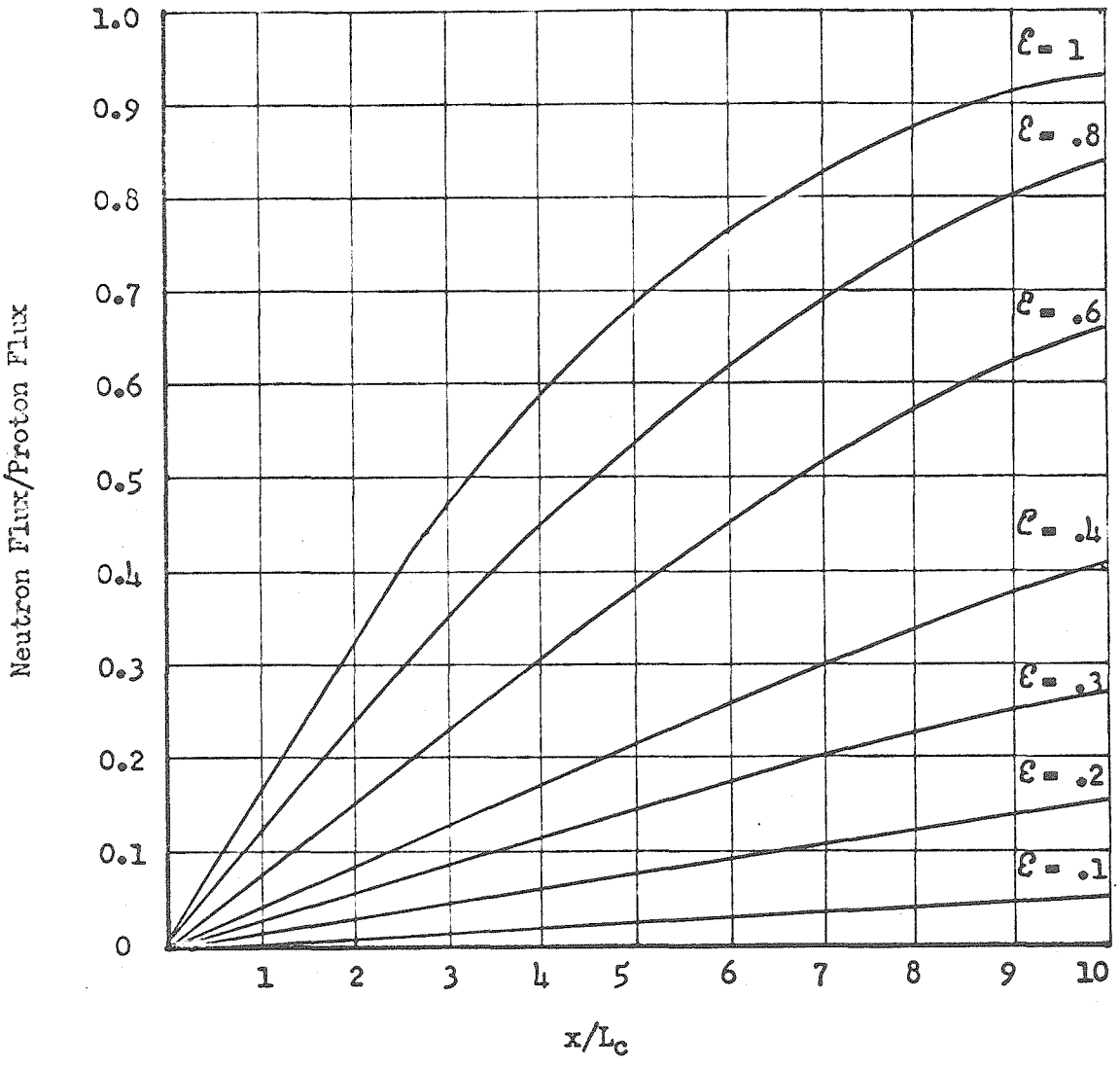

Fig. 15. Ratio of neutrons to protons in the atmosphere.

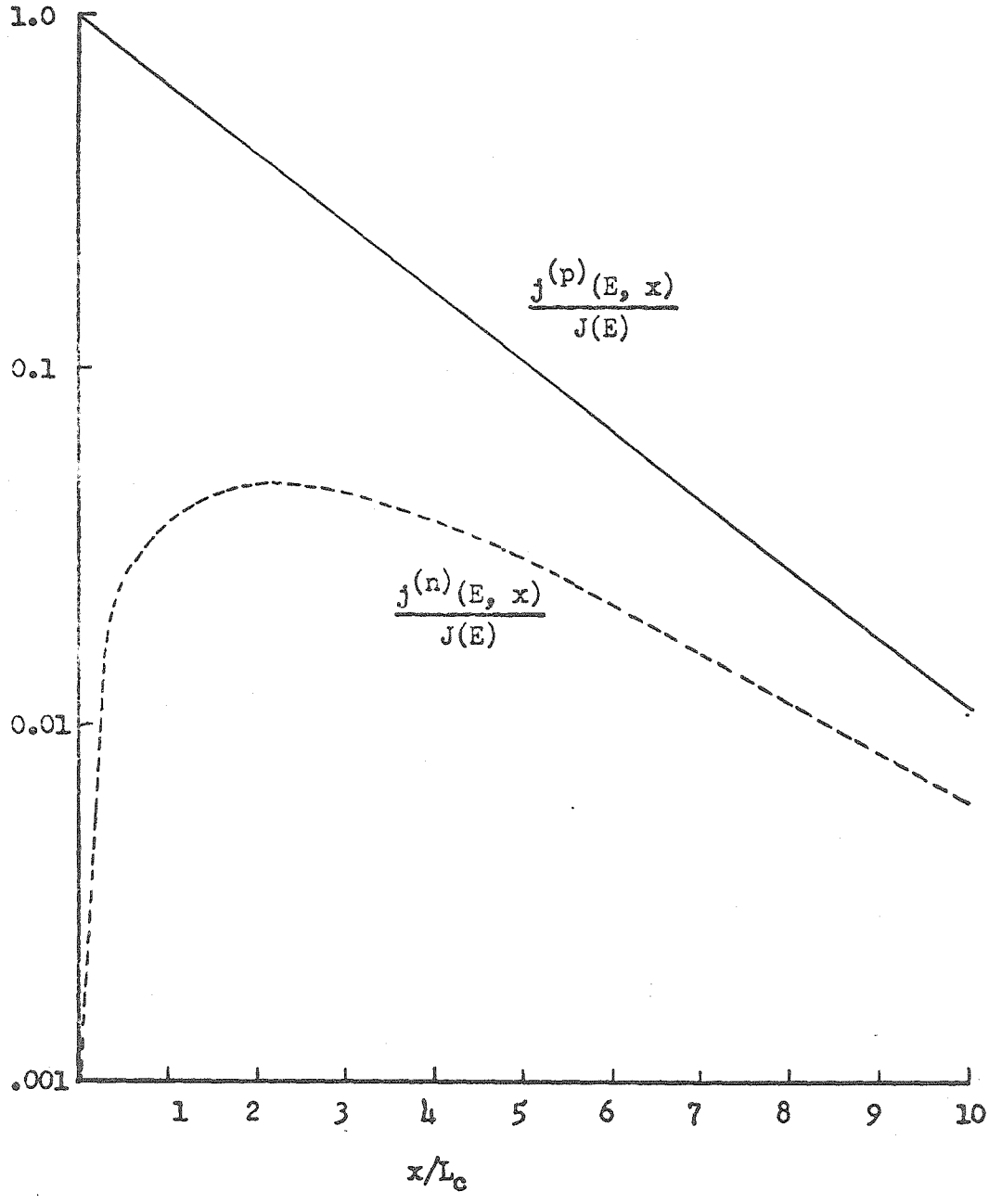

Fig. 16. Flux density of neutrons and protons in the atmosphere for $\mathcal{E} = 0.5$

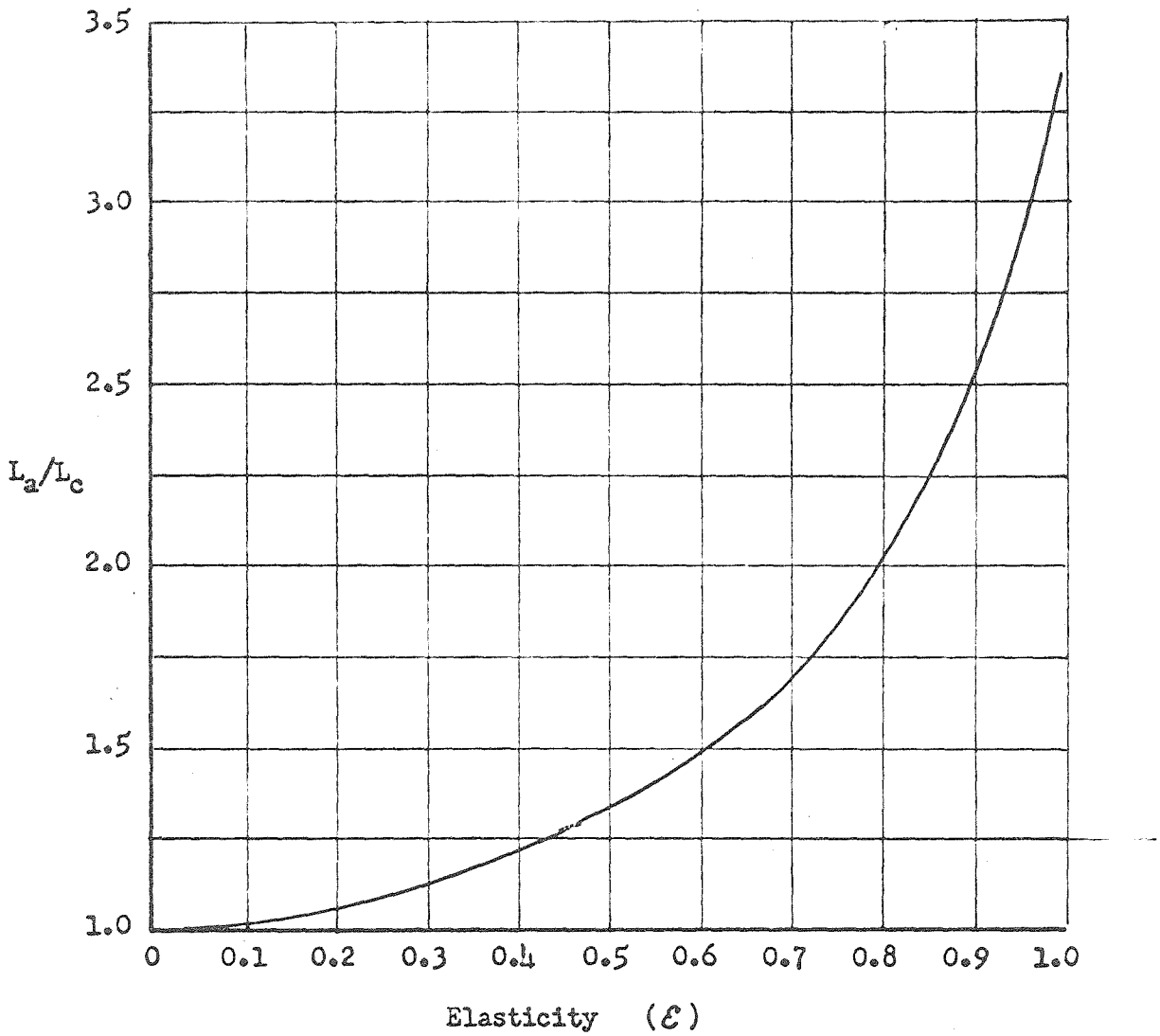

Fig. 17. Ratio of absorption thickness, L_a, to interaction length, L_c, for high energy nucleons in the atmosphere (eq. 69).

APPENDIX A

A. Some Useful Relativistic Relations

Because of the repeated necessity of transforming experimentally measured quantities in the laboratory system to theoretically predicted quantities in the center-of-mass system, a summary of these transformations is included here. For convenience, the velocity of light and the nucleon mass (neglecting the small difference between neutrons and protons) are taken as 1.

Notation: L system refers to the laboratory system.

C system refers to the center-of-mass system.

β = the velocity of a particle in L system.

$\gamma = (1-\beta^2)^{-1/2}$ the total energy of a particle in the L system.

θ_s = angle of emission of a secondary measured from the line of flight of the incident nucleon in the L system.

β', γ', θ_s' are the corresponding quantities in the C system.

β_c = the velocity of the C system.

$\gamma_c = (1-\beta_c^2)^{-1/2}$

$\mathcal{E}$ = the elasticity (Eq. 40).

k = the inelasticity (Eq. 41).

Let A_ν be a four-vector in the L system which transforms via the Lorentz transformation into the four-vector A'_ν in the C system by means of

$$A'_\mu = \sum_\nu a_{\mu\nu} A_\nu \text{ or } A_\mu = \sum_\nu b_{\mu\nu} A'_\nu \qquad \text{(A1)}$$

where

$$a_{\mu\nu} = \begin{pmatrix} \gamma_c & 0 & 0 & i\beta_c\gamma_c \\ 0 & 1 & 0 & 0 \\ 0 & 0 & 1 & 0 \\ -i\beta_c\gamma_c & 0 & 0 & \gamma_c \end{pmatrix} \tag{A2}$$

and

$$b_{\mu\nu} = \begin{pmatrix} \gamma_c & 0 & 0 & -i\beta_c\gamma_c \\ 0 & 1 & 0 & 0 \\ 0 & 0 & 1 & 0 \\ i\beta_c\gamma_c & 0 & 0 & \gamma_c \end{pmatrix} \tag{A3}$$

The momentum-energy four vectors in the L and C system for each of the nucleons (subscript p refers to the incident nucleon, t to the target nucleon) will be

$$\begin{aligned} P_p &= (\sqrt{\gamma_p^2 - 1},\ 0,\ 0,\ i\gamma_p) & P_p' &= (\sqrt{\gamma_p'^2 - 1},\ 0,\ 0,\ i\gamma_p') \\ P_t &= (0,\ 0,\ 0,\ i) & P_t' &= (-\sqrt{\gamma_p'^2 - 1},\ 0,\ 0,\ i\gamma_p') \end{aligned} \tag{A4}$$

Transforming p_p and p_t into p_p' and p_t', and solving the resulting equations gives the following relations between γ_p', γ_p and γ_c (using $\gamma_t' = \gamma_p'$):

$$\gamma_p' = \gamma_c \tag{A5}$$

$$\gamma_p = 2\gamma_c^2 - 1 \tag{A6}$$

Consider a secondary particle of mass η (in terms of $Mc^2 = 1$) emitted with velocity β_s at an angle θ_s with respect to β_c. Its energy-momentum four-vectors in L and C are

$$P_s = (\eta \sqrt{\gamma_s^2 - 1}\cos\Theta_s,\ \eta\sqrt{\gamma_s^2-1}\sin\Theta_s,\ i\eta\gamma_s)$$

$$P_s' = (\eta\sqrt{\gamma_s'^2 - 1}\cos\Theta_s',\ \eta\sqrt{\gamma_s'^2 - 1}\sin\Theta_s',\ 0,\ i\eta\gamma_s') \tag{A7}$$

Transforming p_s' to p_s

$$\tan\Theta_s = \frac{\sin\Theta_s'}{\cos\Theta_s' + \beta_c/\beta_s'}\ \frac{1}{\gamma_c} \tag{A8}$$

and $$\gamma_s = \gamma_c\gamma_s' + [(\gamma_c^2 - 1)(\gamma_s'^2 - 1)]^{\frac{1}{2}}\cos\Theta_s' \tag{A9}$$

If the secondaries come to rest in the C system, $\gamma_s' = 1$ and $\gamma_s = \gamma_c$.

From Eqs. 5 and 6, the total energy of each nucleon in the C system is related to the primary energy in the L system by

$$\gamma_p = 2\gamma_p'^2 - 1 \tag{A10}$$

The maximum energy available for meson production in the C system is the kinetic energy of the two nucleons given by $2(\gamma_p'-1)$. If this energy is entirely converted to mesons, the nucleons will be at rest in the C system and hence their energy in the L system will be $2\gamma_c$. The ratio of the kinetic energy of the secondary nucleons to the primary nucleons in L is thus

$$\mathcal{C} = \frac{2(\gamma_c-1)}{(\gamma_p-1)} = \frac{1}{\gamma_c+1} \tag{A11}$$

and the fraction of the kinetic energy of the primary which is available for meson production is

$$k = 1 - \mathcal{C} = \frac{\gamma_c}{\gamma_c+1} \tag{A12}$$

APPENDIX B

B. Calculation of True Angle of Incidence from Left and Right Views

Let x_t, y_t and z_t be the cartesian coordinates with respect to the axis of the cloud chamber of τ, a point at the tip of an infinitesimal vector having the direction of the incident particle and origin at the intersection of the track and the iron plate. (x_t, y_t and z_t will be the lengths of three vectors which sum to $\overline{0\tau}$). Let y_L and x_L be the coordinates with respect to point 0 of the projection of τ on the x-y plane from the point L. The coordinates of 0 are given by x_o, y_o and z_o.

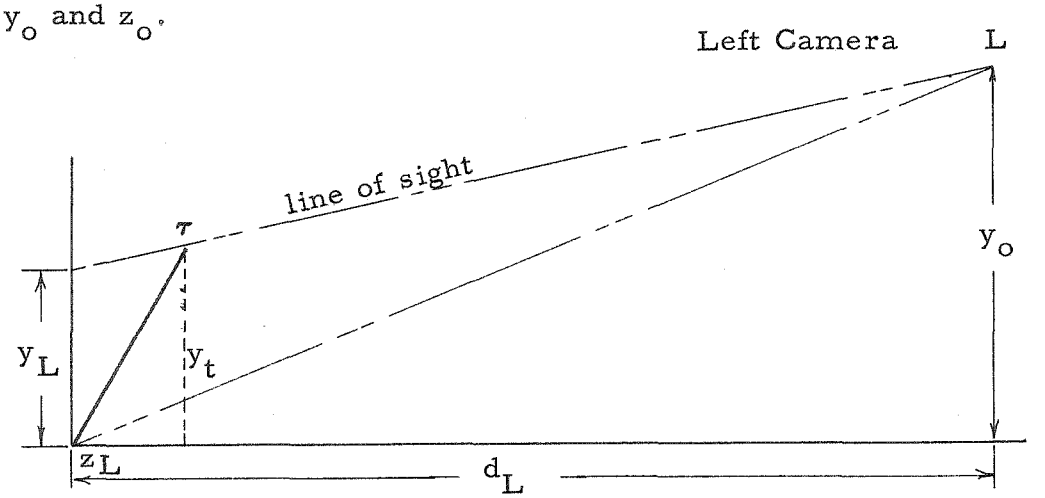

Fig. 19. Projection of True Trajectory on Plane Parallel to y-axis containing line of sight $\overline{0L}$.

From inspection of Fig. 19

$$\frac{z_L}{y_t - y_L} = \frac{d_L}{y_o} \qquad \text{where} \quad d_L = [(d + z_o)^2 + (s+x_o)^2]^{\frac{1}{2}}$$

$$\text{or} \quad y_L = y_t - \frac{z_L y_o}{d_L}$$

From Fig. 18 the relationship between z_L and z_y can be seen to be

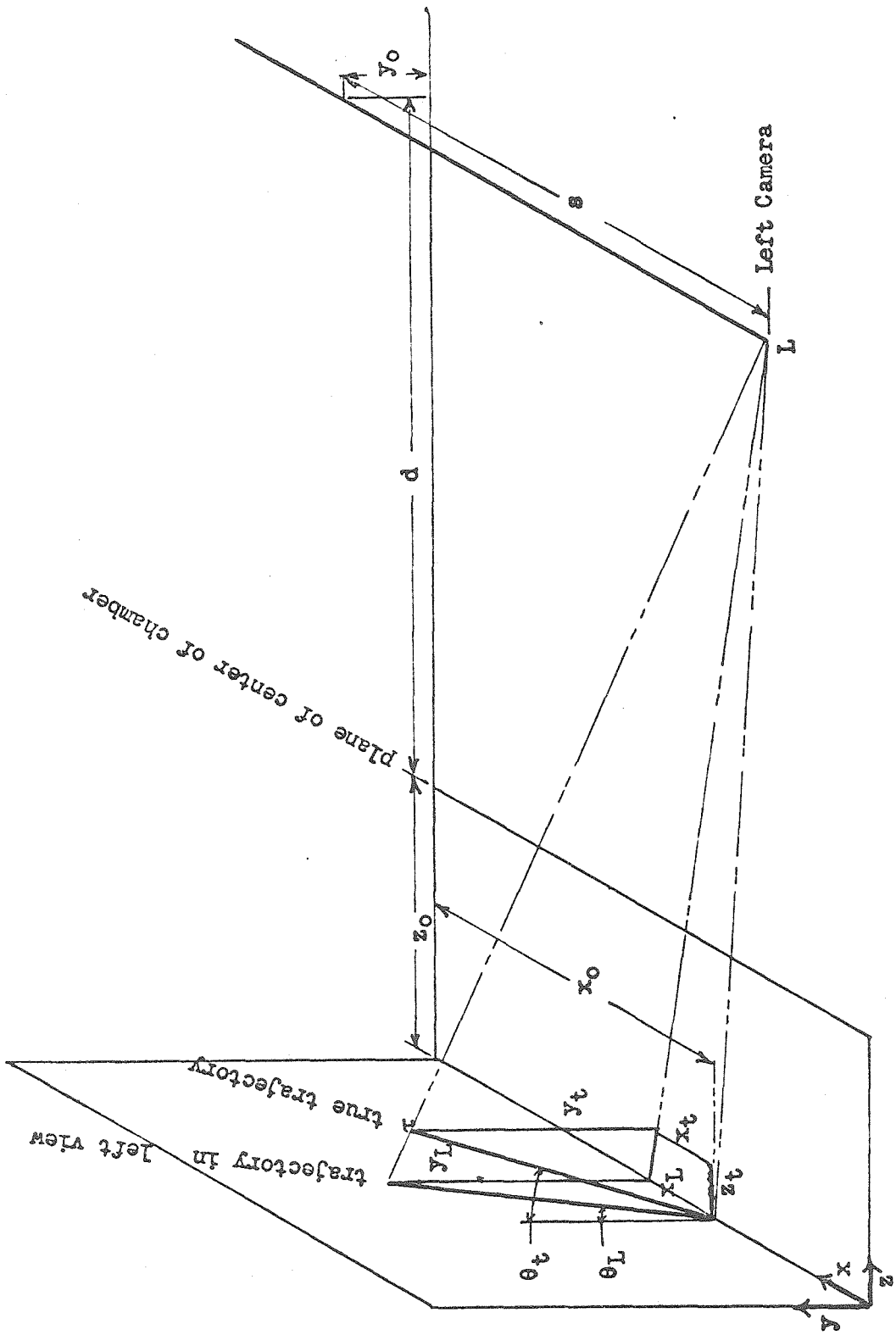

Fig. 19. Projection of true trajectory in left view.

$$z_L = \frac{d_L z_t}{d+z_o} \quad \text{or} \quad y_L = y_t - \frac{z_t y_o}{d+z_o} \tag{B1}$$

By similar reasoning for the right view

$$y_R = y_t - \frac{z_t y_o}{d+z_o} \tag{B2}$$

y_R and y_L, the coordinates of τ in the right and left views are thus identical as they should be.

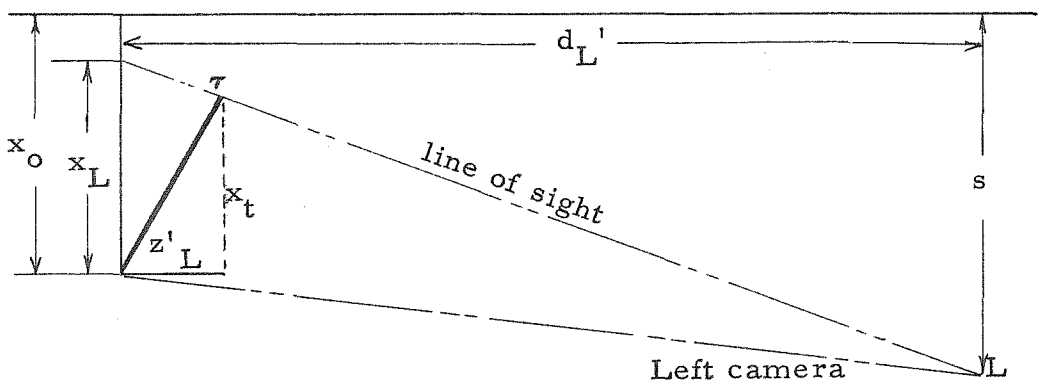

Fig. 20. Projection of True Trajectory on Plane Parallel to x-axis and containing line of sight $\overline{0L}$.

From inspection of Fig. 20

$$\frac{z'_L}{x_L - x_t} = \frac{d'_L}{s-x_o} \quad \text{where } d'_L = [(d+z_o)^2 + y_o^2]^{\frac{1}{2}} \tag{B3}$$

$$\text{or} \quad x_L = x_t + \frac{z_t(s+x_o)}{d+z_o}$$

By similar reasoning for the right view

$$x_R = x_t - \frac{z_t(s+x_o)}{d+z_o} \tag{B4}$$

Solving for x_t, y_t and z_t in Eqs. 2, 3, and 4

$$z_t = \frac{d+z_o}{2s}(x_L - x_R) \tag{B5}$$

$$y_t = y_L + \frac{y_o}{2s}(x_L - x_R) \tag{B6}$$

$$x_t = \frac{1}{2}(x_L + x_R) + \frac{x_o}{2s}(x_L - x_R) \tag{B7}$$

The quantity required is the secant of the true angle between the y axis and $\overline{0\tau}$ given by

$$\sec^2\theta = \frac{x_t^2 - y_t^2 - z_t^2}{y_t^2} = 1 - \frac{x_t^2 - z_t^2}{y_t^2} =$$

$$1 + \frac{\left[\frac{1}{2}(x_L + x_R)\right]^2 + \left[\frac{d + z_o + x_o}{2s}(x_L - x_R)\right]^2 + \frac{x_o}{2s}(x_L^2 - x_R^2)}{\left[y_L + \frac{y_o}{2s}(x_L - x_R)\right]^2} \tag{B9}$$

Because of the large number of tracks to be corrected it is convenient to obtain an approximation to this expression by considering the maximum values of x_o, y_o, z_o, x_t, y_t, and z_t. The following result gives a value of $\sec\theta$ accurate to 5%.

$$\sec^2\theta = 1 + \frac{\left[\frac{1}{2}(x_L + x_R)\right]^2 + \left[\frac{d}{2s}(x_L - x_R)\right]^2}{y_L^2}$$

In terms of the angles measured on the film, $\tan\theta_L = x_L/y_L$ and $\tan\theta_R = x_R/y_R$

$$\sec\theta = \sqrt{1 + \left[\frac{1}{2}(\tan\theta_L + \tan\theta_R)\right]^2 + \left[\frac{a}{2s}(\tan\theta_L - \tan\theta_R)\right]^2} \tag{B10}$$

REFERENCES

1. B. Rossi, High Energy Particles, Prentice Hall
2. Glasser and Shein, Phys. Rev., 90, 218 (1953)
3. Kaplon, Peters and Ritson, Phys. Rev., 85, 900 (1952)
4. Engler, Haber-Schaim and Winkler, Nuovo Cimento, 12, 932 (1954)
5. Glasser, Haskin, Schein and Lord, Phys. Rev., 99, 1555 (1955)
6. Dilworth, Goldsack, Hoang and Scarsi, Nuovo Cimento, 10, 1261 (1953)
7. Costagnoli, Cortini, Franzinetti, Manfrenini and Moreno, Nuovo Cimento, 10, 1539 (1953)
8. Schein, Haskin, Lohrmann and Teucher, Proc. Moscow Cosmic Ray Conf. 1, 6 (1960)
9. Lord, Fainberg, and Schein, Phys. Rev., 80, 970 (1950)
10. Peirels, Trans. Roy. Soc. (London) 149, 124 (1935)
11. D. Davis, T. Hoang, and M. Kaplon, Phys. Rev., 106, 1049 (1957)
12. W. Alford and R. Leighton, Phys. Rev., 90, 622 (1953)
13. M. S. Bartlett, Phil. Mag., 44, 249 (1953)
14. R. A. Fisher, Trans. Roy. Soc. (London) 222, 309 (1922)
15. Worthington and Geffner, Treatment of Experimental Data, Pgs. 238ff, Wiley (1943)
16. Hald, Statistical Theory, Pgs. 522ff, Wiley (1952)
17. Brunk, Mathematical Statistics, Pgs. 199, Ginn (1960)
18. A. E. Brenner and R. W. Williams, Phys. Rev., 106, 1020 (1957)
19. Alexander and Yekutreli, Nuovo Cimento, 9, 108 (1961)
20. Fernbach, Serber and Taylor, Phys. Rev., 75, 1352 (1949)
21. Hahn, Ravenhall and Hofstadter, Phys. Rev., 101, 1131 (1956)
22. R. Hofstadter, Rev. Modern Physics, 28, 214 (1956)
23. R. Hofstadter, Ann. Rev. Nuc. Phys., 7, 231 (1957)
24. U. Meyer-Berkhout, K. W. Ford and A.E.S. Green, Ann. Phys., 8 119 (195)

25. R. H. Helm, Phys. Rev., 104, 1466 (1956)

26. Longo, Helland, Hess, Moyer and Perez-Mendez, Phys. Rev. Letters, 3, 568 (1959)

27. Bowen, Di Crato, Moore and Tagliaferri, Nuovo Cimento, 9, 908 (1958)

28. Hand-Book of Physics, p. 9-208, McGraw-Hill (1960)

29. Chen, Lewitt, Shapiro, Phys. Rev., 99, 857 (1955)

30. Coor, Hill, Hornyck, Smith and Snow, Phys. Rev., 98, 1369 (1955)

31. Sinha and Das, Phys. Rev., 105, 1587 (1957)

32. J. H. Atkinson, Ph.D. Thesis, UCRL - 8966 (1959)

33. Ashmore, Cocconi, Diddens and Wetherell, Phys. Rev. Letters, 5, 576 (1960)

34. Wilnot N. Hess, Phys. Rev., 30, 368 (1958)

35. Dzhelepov, Moskalev and Medved, Doklady Akad. Nauk., S.S.S.R., 104, 380 (1955)

36. N. P. Bogachev and I. K. Vzorov, Diklady Akad. Nauk., S.S.S.R., 99, 931 (1954)

37. Smith, McReynolds and Snow, Phys. Rev., 97, 1186 (1955)

38. Shapiro, Leavitt, and Chen, Phys. Rev., 95, 663 (1954) and Chen, Leavitt and Shapiro, Phys. Rev., 103, 211 (1956)

39. Batson, Culwick, Reddiford, Walker, Proceedings, European Organization for Nuclear Research, Geneva, 1956 (CERN Symposium, Geneva, 1956) Vol. II, p. 344

40. Morris, Fowler, and Garrison, Phys. Rev. 103, 1472 (1956)

41. Hughs, March, Muirhead and Lock, Proceedings, European Organization for Nuclear Research, Geneva, 1956 (CERN Symposium, Geneva, 1956) Vol. II, p. 344

42. Fowler, Shutt, Thorndike and Whittemore, Phys. Rev. 103, 1497 (1956)

43. Block, Harth, Cocconi, Hart, Fowler, Shutt, Thorndike and Whittemore, Phys. Rev. 103, 1484 (1956)

44. Wright, Saphir, Powel, Maenchen and Fowler, Phys. Rev. 100, 1802A (1955)

45. N. P. Bogachev, S. A. Bunzatov, I. M. Gramenitski, V. B. Lzubinov, Yu. P. Merekov, M. I. Podgoretsky, V. M. Siderov and D. Tuvdendozh, J. Exptl. Theoret. Phys. (U.S.S.R.) 37, 1225 (1959) (Translation: Soviet Physics - J.E.T.P. 37 (10), 872, (1960)

46. G. von Dardel, D. H. Frisch, R. Mermod, R. H. Melburn, P. A. Piroue, M. Vivarzent, G. Weber and K. Wenter, Phys. Rev. Letters, 5 333m (1960)

47. Bogachev, Bunzatov, Merekov and Sidorov, Dokl. Akad. Nauk. S.S.S.R. 121, 617 (1958); Soviet Physics, - Diklady 3, 785 (1959)

48. R. Marshak, Meson Physics, 273 ff, McGraw-Hill (1952)

49. Shein, Haskin, Lohrman and Tencher, Proc. of Moscow Cosmic Ray Conf., 6, (1960)

50. Hanson and Fretter, Phys. Rev., 118, 812 (1960) and Proc. of Moscow Cosmic Ray Conf., 136 (1960)

51. Montanet, Newth, Petrucci, Salmeron and Zichichi, Nuovo Cimento, 17, 166 (1960)

52. Barkow, Chamary, Hoskins, Jain, Lohrman, Tencher and Shein, Phys. Rev., 122, 617 (1961)

53. E. W. Cowan, From a paper presented at 1960 Rochester Conference on High Energy Physics